ıbric, exemplified in metamorphic rocks,
. If the orientation of the fabric elements
nts have a preferred orientation, the fab-
ic is *packing* – the spacing or density pat-
ıner by which grains are packed controls
a sediment. Discussions of packing may
)65), and Blatt et al. (1972).
stic rocks also includes *dimensional* and
ation is determined by particle shape.
: dimensionally oriented although they
mensional orientation is also achieved
ıary lapilli become flattened upon im-
ırds and pumice deform by compaction
al fragments that come to rest at tem-
: contained ferromagnetic minerals de-
ıgnetism (magnetic orientation). Thus,
tool for distinguishing hot pyroclastic
elded spatter from ash falls or pumice-
tures (Aramaki and Akimoto, 1957;
d Mullineaux, 1973).

# *Chapter 6* Subaerial Fallout Tephra

The transport modes of subaerial fallout tephra are (1) by ballistic trajectory and (2) by turbulent suspension. Energy is supplied initially to fragments by the eruption and later by wind. Tephra that falls from the atmosphere onto land is called *subaerial fallout* or airfall tephra. Tephra deposited in standing water is called *subaqueous fallout* tephra and includes (1) submarine or marine tephra, and (2) sublacustrine tephra. Subaqueous fallout tephra originating from eruptions on land is discussed separately (Chap. 7) from pyroclastic materials originating wholly beneath water (Chap. 10). Island arc and oceanic island flank environments generally include both kinds.

Parameters useful for identifying the airfall process are rock associations, geometry of an entire deposit, and the sorting and grading in individual layers (Table 6-1). Field mapping of lateral distribution, isopach maps and size parameters, in particular maximum sizes of clasts, are especially useful. Such data are fundamental for further calculations regarding eruptive centers, ancient wind patterns, volume and shape of magma chambers, vent radius, dynamics and height of eruption columns, terminal velocity of ballistic fragments, and eruptive energy.

Wide-spread ash layers are important stratigraphic marker horizons because they are deposited within a short period of time. The fields of tephrochronology and tephrostratigraphy are concerned chiefly with dating and correlating geologically young ash deposits (Chap. 13). Airfall tephra also is increasingly studied to analyze eruptive processes. We concentrate here on some of the descriptive parameters of tephra sheets and their geologic and volcanologic interpretations.

Vertically directed subaerial eruptions are characterized by the formation of an eruption column consisting of pyroclasts, expanding gases, and entrained air. Size and density sorting of particles occurs within the column, because particles of least settling velocity are carried to greater heights and spread over greater distances than those with large settling velocities. Many eruption columns consist of a lower gas-thrust region, and an upper convective-thrust region (Chap. 4) in which thermal energy converts to mechanical energy, thus developing an expanding turbulent column (eruption cloud) which may rise to great heights. Eruption clouds are commonly pushed laterally *en masse* by the wind (Fig. 6-1), but individual fragments within the cloud are suspended by turbulence. Some eruptions, however, show multiple behavior, for example the May 18, 1980 Mount St. Helens eruption with a directed blast as well as vertical columns which produced complex patterns of ash deposition (Waitt and Dzurisin, 1981).

Three dominant threshold settling velocity values for a given set of conditions affect the distribution and sorting of airborne tephra: (1) fragments with large settling velocities follow ballistic trajectories that are little affected by wind and only

**Table 6-1.** Characteristics of subaerial fallout deposits

*Comment:* The characteristics of subaerial fallout deposits are highly variable depending upon the kind of eruption (e.g. Strombolian, Plinian, etc.), changes in eruptive style during an eruption, composition, and distance to source. Some of the features listed below are generally applicable, but others can only be used for certain eruptive types.

*Distribution (fallout pattern) and thickness*

Circular or fan-shaped (regular to irregular) distribution with respect to source. Secondary thickness maxima may occur far downwind.
Flat wedges that decrease systematically in thickness along fan axes. Some have displaced or multiple thickness maxima
Thickness may be skewed to one side, perpendicular to fan axis.
Azimuth of fan axis may change with distance from source.
Apex of fan axis may not be on volcano (e.g., Mount St. Helens).

*Structures*

Plane-parallel beds drape over gentle topography and minor surface irregularities. Ash layers wedge out against cliffs or other steep surface irregularities.
Laminations and thicker beds reflect compositional changes or textural changes; either of these may cause overall color changes.
Minor lenticularity may occur close to source.
Grading may be both normal and reverse in various combinations depending upon variations in wind and/or eruption energy, vent radius or eruption column density.
Reverse grading in beds on cinder cones and other steep slopes commonly develops by downslope rolling or sliding of dry granular material.
Fabric in beds is commonly isotropic because elongate fragments are uncommon. Exceptions: phenocrysts such as biotite, amphibole, etc. and platy shards.
Bedding planes may be sharp if there are abrupt changes in eruptive conditions, wind energy or directions, or in composition.
Bedding planes are distinct where deposition is on weathered or erosional surfaces, or different rock types. May be gradational if deposition is slow by small increments so that bioturbation, wind reworking, and other soil-forming processes dominate.

*Textures*

Sorting: moderate to good: Inman parameters, $\sigma_\phi$, 1.0 to 2.0 most common. This applies to relatively coarse-grained as well as to fine-grained tephra.
Median diameter, $Md_\phi$: Highly variable depending upon type of volcanism and distance to source. $MD_\phi$ commonly $-1.0$ to $-3.0$ (2 mm to 8 mm) or smaller (phi values) close to source, but farther from source, $Md_\phi$ may vary from 0.0 (1 mm) to 3.0 (1/8 mm) or more.
Size and sorting parameters vary geometrically with distance in single layers.

*Composition*

Any composition, but silicic or intermediate fallout more widespread than mafic fallout, due to usually greater explosivity and discharge rate of the eruptions.
Intermediate composition is commonly associated with large composite volcanoes.
Mafic composition commonly associated with scoria cones and lava flows.
Bulk composition generally becomes slightly more silicic away from source due to eolian fractionation.

*Rock Associations and Facies*

Close to source (within vent or on steep volcano slopes): lava flows, pyroclastic flows, domes, pyroclastic tuff breccias, avalanche deposits and debris flows.
Intermediate to source: coarse-grained tephra, some lava flows, pyroclastic flows, ash falls and reworked fluvial deposits. The coarser-grained pyroclastic deposits gradually decrease, and reworked pyroclastic deposits gradually increase away from source.
Far from source: Fallout tephra, most easily recognized in marshy, lacustrine, wind blown environments. Rock associations depend on environment of deposition; no co-eval coarse-grained pyroclastic rocks or lava flows.

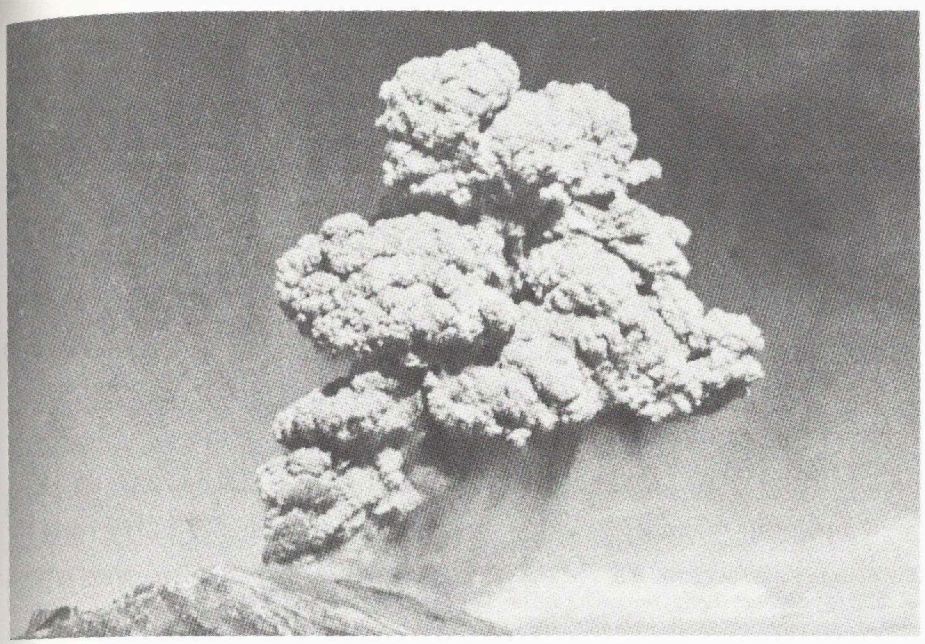

**Fig. 6-1.** Eruption of Mt. Asama, Japan (1:09 p.m., December 5, 1958) illustrating fallout of particles from a turbulent eruption column. The turbulent column is being pushed *en masse* by the wind. (Courtesy of I. Murai)

slightly by the expanding eruption cloud, (2) particles suspended by turbulence in the eruption cloud but which are too heavy to be suspended by atmospheric winds and (3) those light enough to be suspended by wind independently of the eruption cloud. Wind may modify the trajectories of all but the largest fragments; fragments held in turbulent suspension within an eruption cloud begin to fall according to their settling velocities as the energy within the cloud dissipates; fragments with fall velocities that are small compared to wind strength may circle the earth many times before settling (Lamb, 1970). It is becoming increasingly clear, however, that the very small particles commonly become agglutinated by moisture in eruption clouds to form accretionary lapilli which are larger and heavier than the individual particles that make up the lapilli. Thus, large volumes of very small particles may fall out prematurely (Brazier et al., 1982; Carey and Sigurdsson, 1982). Wide dispersal of airborne tephra is strongly dependent upon wind vectors at different altitudes (Baak, 1949; Waitt and Dzurisin, 1981).

The sorting of tephra deposits either by size or density is rarely perfect. The finest of particles, for example, may (1) fall as accretionary lapilli along with large particles, (2) come down in rain drops ("rain flushing"), (3) become trapped within a densely crowded fall of coarse-grained ash and lapilli or (4) at long distances, form porous clusters by mechanical interlocking and electrostatic attraction which fall like snow flakes (Sorem, 1982). Thus, large and small particles may be deposited together within any single layer close to the source. With the exception of

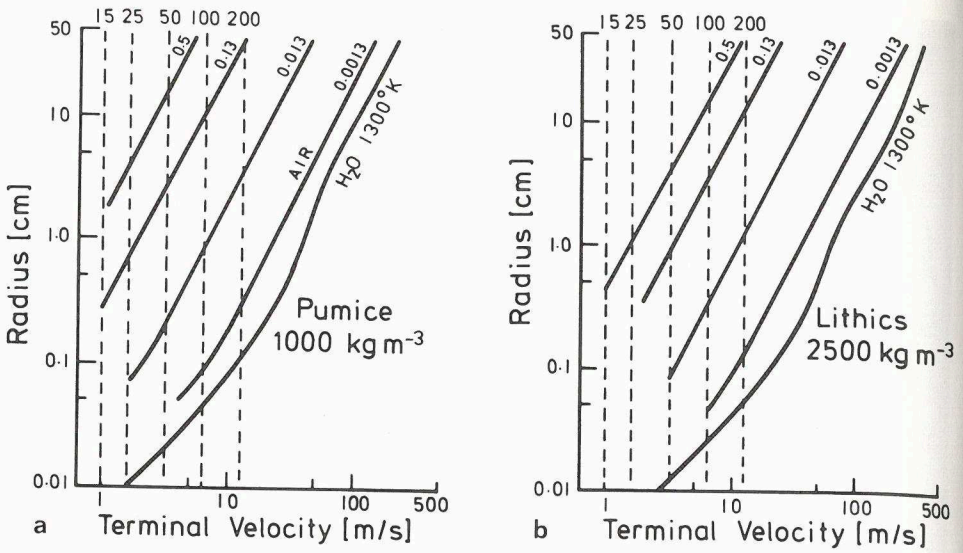


**Fig. 6-2 a, b.** Terminal velocities of **a** pumice and **b** lithic particles of different sizes (to 50 cm) in fluids of different densities. *Lower two curves* are for air at room temperature and steam at 1,300 K. *Vertical dashed lines* represent shear stress velocities of 15 to 200 m $s^{-1}$ and a drag coefficient of 0.01 to define particle sizes that can be suspended in pyroclastic flows at specific velocities. (After Sparks et al., 1978)

aberrations caused by premature fallout from particle agglutination, however, maximum particle sizes and sorting coefficients decrease in a general way as distance from the source increases.

The fall velocities of large ballistic fragments in air have been investigated by Minakami (1942), Fudali and Melson (1972), Chouet et al. (1974) and others; those of smaller fragments by Walker et al. (1971), Wilson (1972) and Wilson and Huang (1979) in air, and in water by Fisher (1965) (Chap. 7). Graphs useful for plotting terminal settling velocities of pumice and lithic fragments in air are presented by Sparks et al. (1978) (Fig. 6-2). Settling velocity data derived from grain size data has been used to construct isopleth maps to estimate eruption column heights and mean wind velocity, and to estimate intensity (mass emission rate of material) as determined from grading characteristics of Plinian deposits (Walker, 1980, Fig. 2 and p. 77, 81).

## Components of Subaerial Fallout

Three main types of tephra components must be distinguished when considering size-distance parameters and therefore compositional variations in tephra (Walker, 1971): crystals, lithic or dense vitric fragments, and pumice – including glass shards (Chap. 5). These different components generally occur in different but overlapping grain size ranges leading to pronounced lateral changes in the overall composition of an ash layer (Walker and Croasdale, 1971; Lirer et al., 1973; Booth et

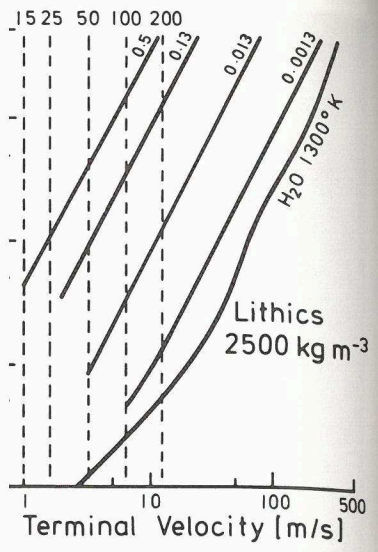


cles of different sizes (to 50 cm) in fluids
ıperature and steam at 1,300 K. *Vertical*
¹ and a drag coefficient of 0.01 to define
fic velocities. (After Sparks et al., 1978)

ɔarticle agglutination, however,
lecrease in a general way as dis-

in air have been investigated by
ıet et al. (1974) and others; those
ɔn (1972) and Wilson and Huang
p. 7). Graphs useful for plotting
agments in air are presented by
ıta derived from grain size data
ıte eruption column heights and
ıss emission rate of material) as
n deposits (Walker, 1980, Fig. 2

distinguished when considering
onal variations in tephra (Wal-
ts, and pumice – including glass
ɛrally occur in different but over-
teral changes in the overall com-
1971; Lirer et al., 1973; Booth et

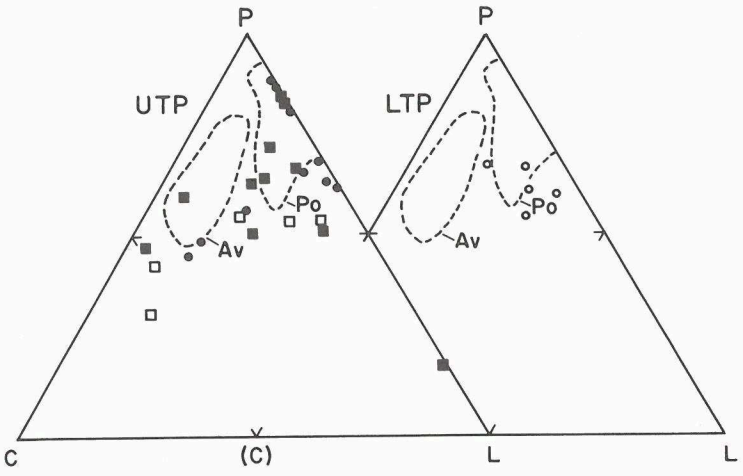


**Fig. 6-3.** Ternary diagrams of pumice (*P*), crystals (*C*) and lithics (*L*) for Upper Toluca Pumice (*UTP*) and Lower Toluca Pumice (*LTP*), Mexico. *Solid circles* on UTP triangle represent the Lower Member; *open squares* and *solid squares* represent the different stratigraphic parts of the Upper Member. *Dashed lines* enclose fields of Avellino (*Av*) and Pompeii (*Po*) pumice deposits of Somma-Vesuvius (Lirer et al. 1973). (After Bloomfield et al., 1977)

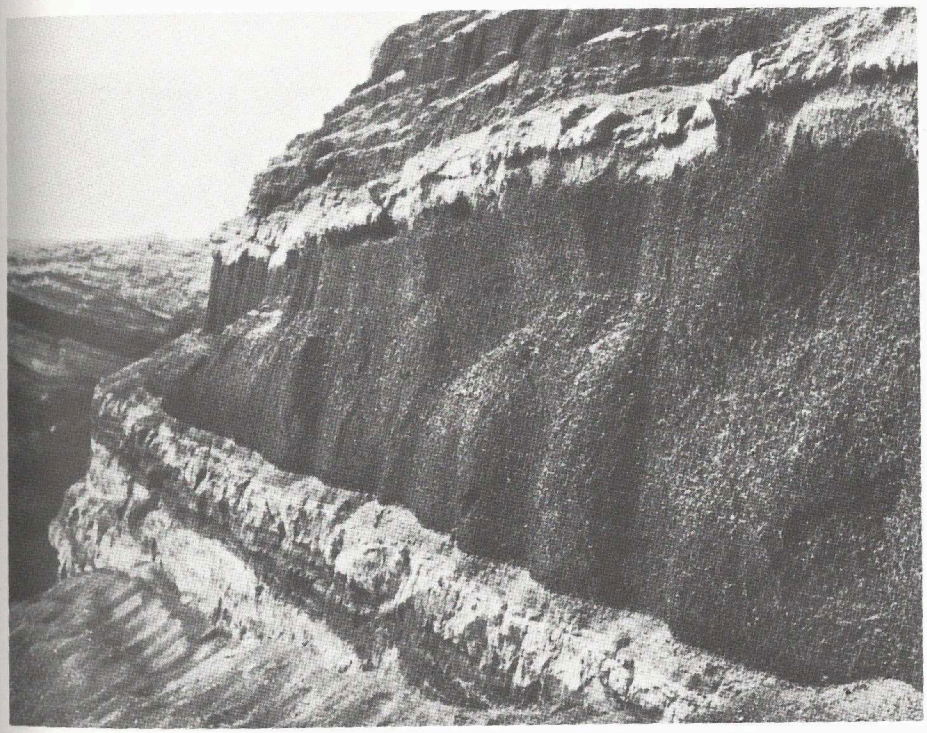

**Fig. 6-4.** Basaltic Plinian fallout lapilli forming a relatively homogeneous bed 1 m thick, becoming bedded in its upper part. Late Quarternary scoria cone (Eifel, Germany). (From Schmincke 1977a)

al. 1978). Tephra from Plinian eruptions may be characterized from ternary diagrams (Fig. 6-3).

We distinguish here between basaltic and felsitic composition of essential tephra particles to contrast end member varieties in a rather simplified scheme. Close to the source, basaltic fallout tephra deposits consist of vesicular to dense lapilli with minor ash and highly variable proportions of bombs and blocks (Figs. 6-4, 6-5) Toward the vent, they become increasingly welded and may grade into agglutinates (Fig. 6-6). An origin by phreatomagmatic processes is likely if the tephra includes large amounts of lithic components associated with abundant fines, an increase in sorting and pronounced bedding.

Felsitic Plinian fallout deposits are much more widely dispersed than those of basaltic composition. Angular pumice lapilli (Fig. 6-7) interspersed with lithic fragments occur in discrete layers or with gradational contacts (Fig. 6-8). Bedding is defined by changes in grain size and composition. A well-sorted matrix of ash-sized crystals, pumice and shards generally forms a minor part of such deposits. Felsitic tephra deposits with overall much finer grain size than pumice-rich Plinian tephra may be attributed to the interaction of water and silicic magma (phreatoplinian) (Self and Sparks, 1978). Most unusual are carbonatite tuffs (Dawson, 1962; Hay, 1978; Keller, 1981). Some resemble limestone beds and calcrete of nonvolcanic origin.

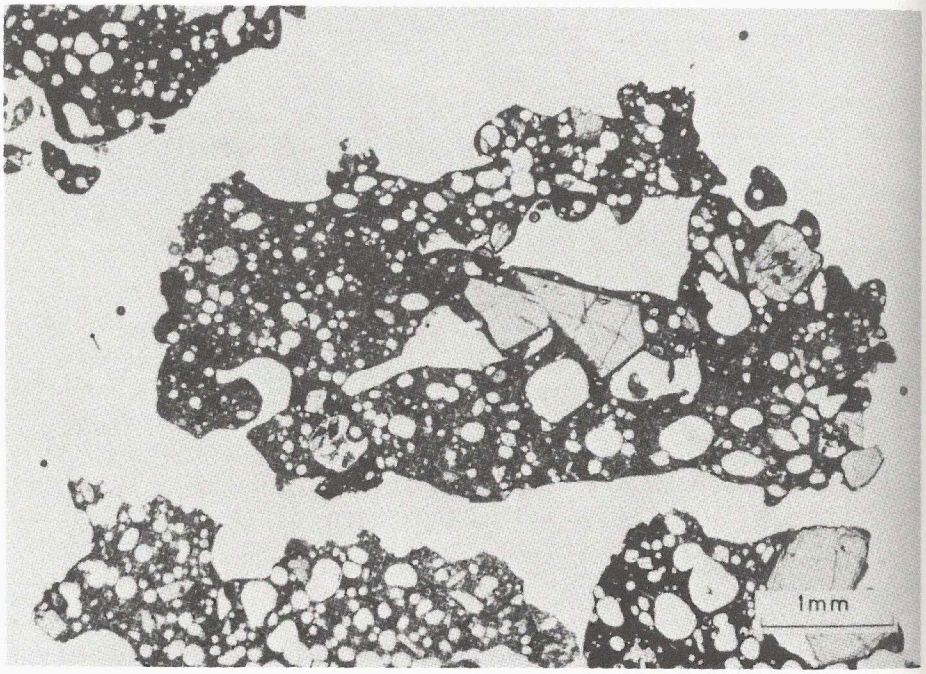


**Fig. 6-5.** Photomicrograph of lapilli of Fig. 6-4. Note irregular shape of lapilli with round smooth edges and clinopyroxene phenocrysts

ıaracterized from ternary dia-

ɜitic composition of essential
ın a rather simplified scheme.
ɜ consist of vesicular to dense
ns of bombs and blocks (Figs.
.y welded and may grade into
ıatic processes is likely if the
.ssociated with abundant fines,

widely dispersed than those of
7) interspersed with lithic frag-
contacts (Fig. 6-8). Bedding is
well-sorted matrix of ash-sized
r part of such deposits. Felsitic
ıan pumice-rich Plinian tephra
ɜilicic magma (phreatoplinian)
tite tuffs (Dawson, 1962; Hay,
ınd calcrete of nonvolcanic or-


hape of lapilli with round smooth edges

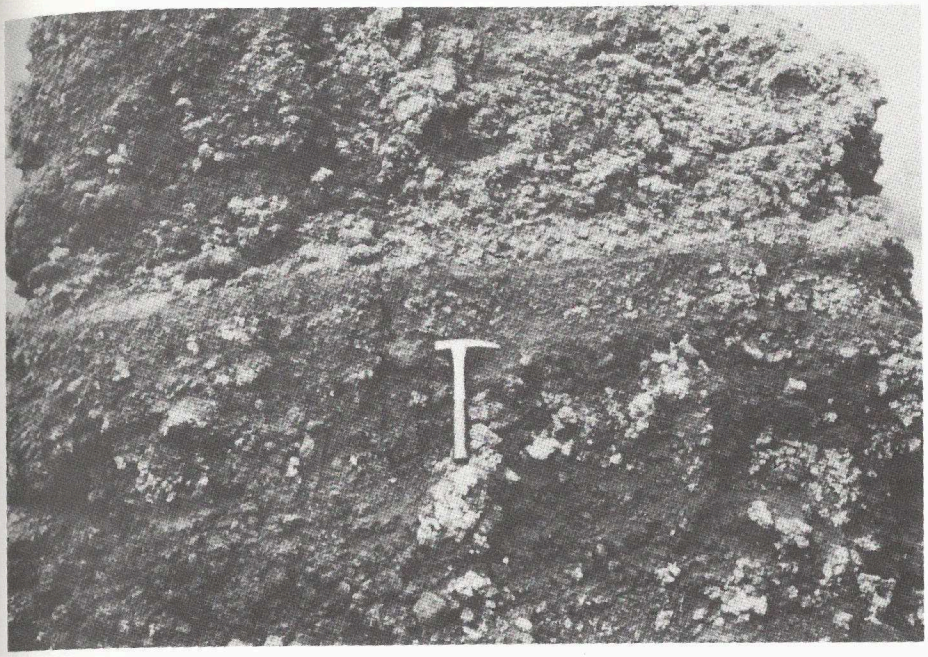

**Fig. 6-6.** Basaltic fallout spatter (agglutinates) at crater rim of Vesuvius (Italy)

**Fig. 6-7.** Trachytic fallout pumice deposit showing very angular lapilli (3 to 5 cm in diameter) and absence of fine matrix. Fogo volcano (São Miguel, Azores)

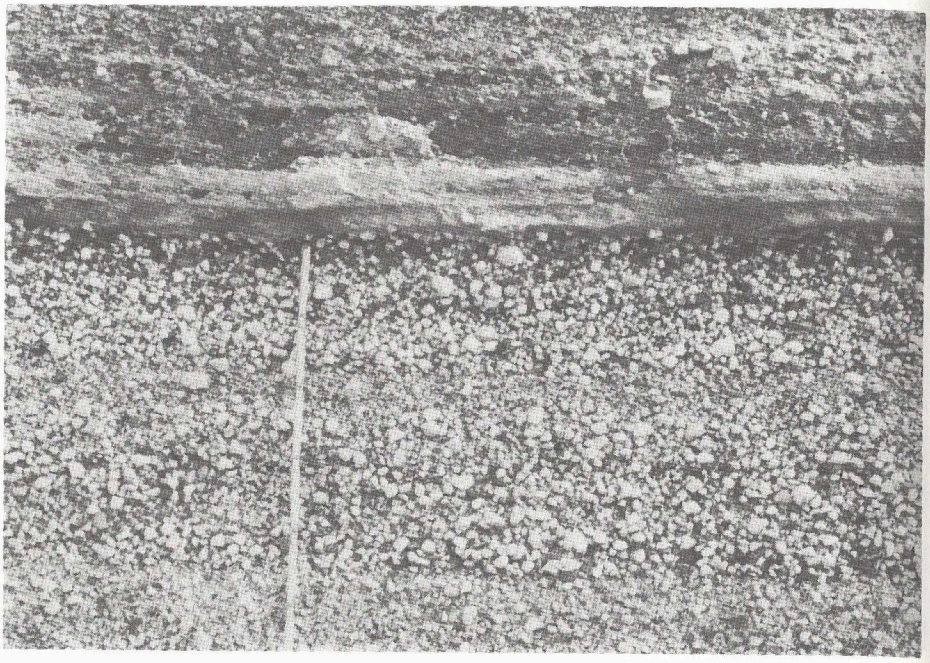

**Fig. 6-8.** Phonolitic Plinian fallout tephra showing enrichment in Devonian slate fragments below surge deposits. Quaternary Laacher See tephra (Eifel, Germany). Scale in 10-cm intervals

## Areal Distribution

### Distribution and Thickness

Fallout tephra sheets are distributed in two end-member patterns with many variations; circular patterns form from rather low eruption columns during calm winds, and elliptical or fan-shaped patterns from high eruption columns that encounter strong unidirectional winds. The most characteristic pattern of single tephra sheets is fan-shaped (Eaton, 1964) with the apex at or near the source. Multicomponent sheets radiate from a common source or overlap with slightly different distribution trends, depending on shifting wind directions (Fig. 6-9). Contemporaneous sheets can be distributed in opposite directions by contrasting winds at different altitudes (Fig. 6-10). Unusually powerful eruptions give rise to sheets easily recognizable 1000 km or more from their source (Fig. 6-11). The ash from such eruptions may be dispersed world-wide, extending far beyond the recognized limits of the dispersal fan, as was illustrated by the May 18, 1980 eruption of Mount St. Helens, Washington (Lipman and Mullineaux, 1981).

Fallout tephra sheets tend to be gentle wedges that systematically thin along an axis away from the source, and are best defined by an isopach map constructed from numerous thickness measurements. In detail, differential compaction, contemporaneous erosion and local topographic irregularities may introduce errors (Aramaki, 1963; Nairn, 1972; Walker, 1980). The source is inferred to lie within

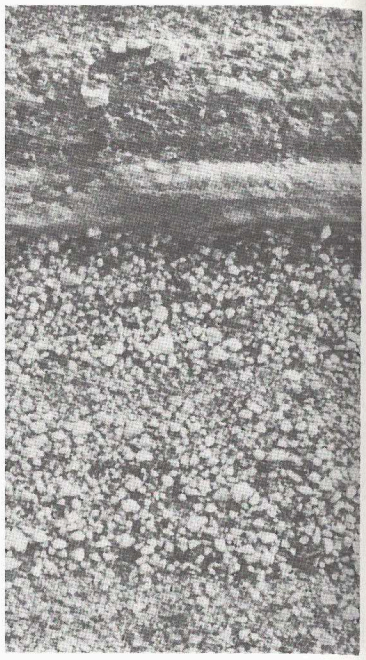

n Devonian slate fragments below surge
e in 10-cm intervals

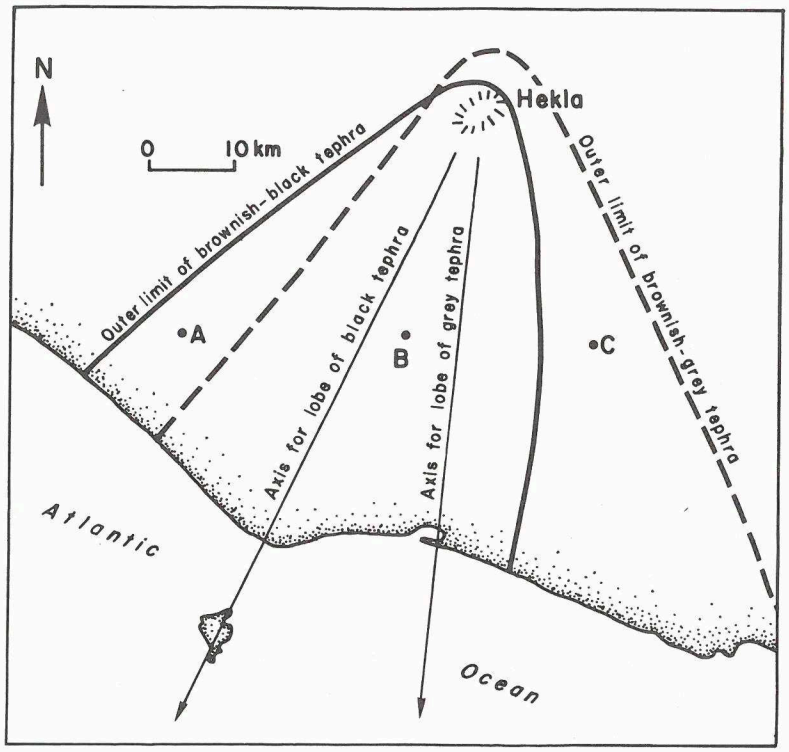


**Fig. 6-9.** Black and gray tephra fans from 1947 Hekla eruption deposited one-half hour apart. The layer at point *A* is dark andesitic tephra and at *C* it is light-colored and dacitic. The andesitic tephra overlies dacitic tephra at *B*. (After Thorarinsson, 1954)

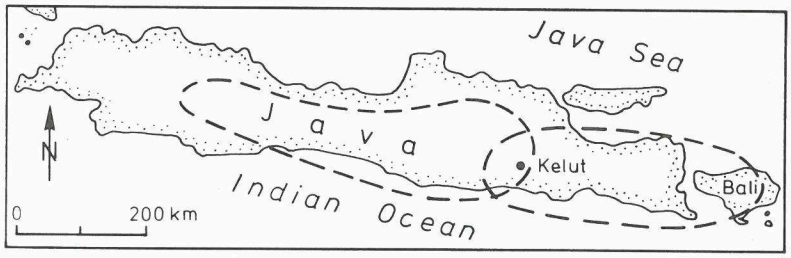


**Fig. 6-10.** Map of Java showing distribution of fallout tephra from the 1919 eruption of Kelut. (After Wilcox, 1959)

ember patterns with many vari-
eruption columns during calm
n high eruption columns that
characteristic pattern of single
apex at or near the source. Mul-
or overlap with slightly differ-
l directions (Fig. 6-9). Contem-
ections by contrasting winds at
eruptions give rise to sheets eas-
(Fig. 6-11). The ash from such
ar beyond the recognized limits
y 18, 1980 eruption of Mount
, 1981).
that systematically thin along
by an isopach map constructed
, differential compaction, con-
gularities may introduce errors
source is inferred to lie within

the maximum thickness contour, but caution must be exercized because the maximum might be displaced downwind (Walker, 1980; Sarna-Wojcicki and Shipley et al., 1981; Waitt and Dzurisin, 1981), or more than one maximum may occur within a single sheet (Fig. 6-12) (Larsson, 1937; Bogaard, 1983). Recent data suggest that displaced maxima may be more common than previously supposed, and that de-

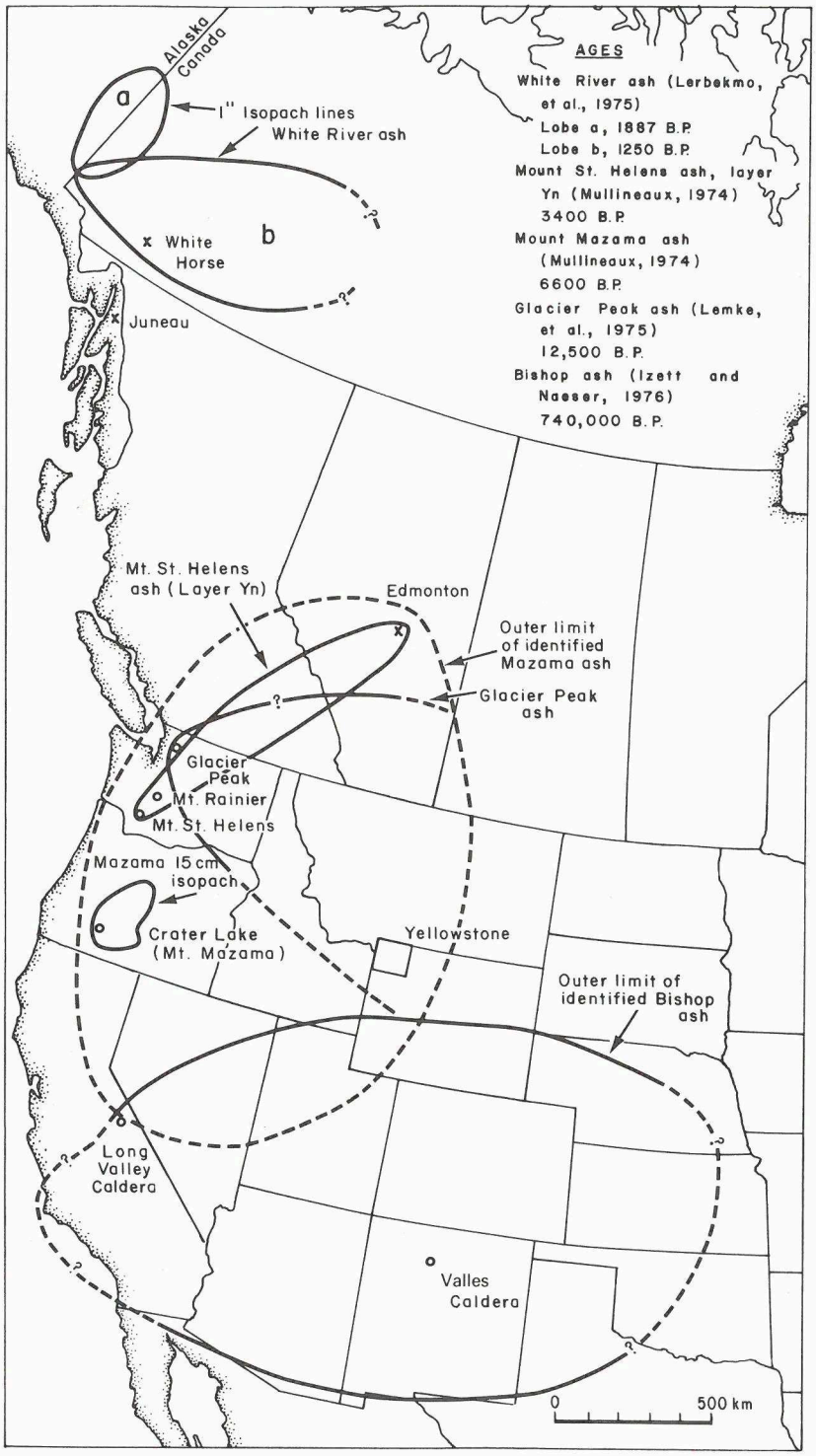
Alaska
Canada
a
1" Isopach lines
White River ash
x White Horse
b
Juneau
AGES
White River ash (Lerbekmo, et al., 1975)
Lobe a, 1887 B.P.
Lobe b, 1250 B.P.
Mount St. Helens ash, layer Yn (Mullineaux, 1974)
3400 B.P.
Mount Mazama ash (Mullineaux, 1974)
6600 B.P.
Glacier Peak ash (Lemke, et al., 1975)
12,500 B.P.
Bishop ash (Izett and Naeser, 1976)
740,000 B.P.
Mt. St. Helens ash (Layer Yn)
Edmonton
Outer limit of identified Mazama ash
Glacier Peak ash
Glacier Peak
Mt. Rainier
Mt. St. Helens
Mazama 15 cm isopach
Crater Lake (Mt. Mazama)
Yellowstone
Outer limit of identified Bishop ash
Long Valley Caldera
Valles Caldera
0
500 km

Fig. 6-11

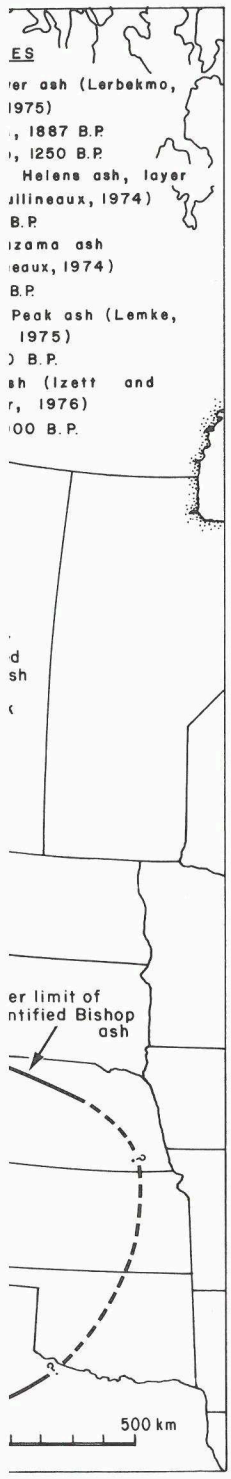


Fig. 6-11

termining tephra volumes based upon the near-source exponential thinning of deposits to large distances must be questioned (Brazier et al., 1983).

With fan-shaped sheets, source may be inferred by projection of the axis but must be done with care because fan axes may curve, as illustrated at Laacher See, Germany (Bogaard, 1983), where fan axes bend at about 3 km from source (Fig. 6-13). Sections at right angles to the axes of elliptical fans may be steeper on one side than on the other (Suzuki et al., 1973). Asymmetry of single tephra sheets is caused by different wind velocities and directions at different altitudes imposed upon an eruption column of fluctuating heights (Fisher, 1964 b).

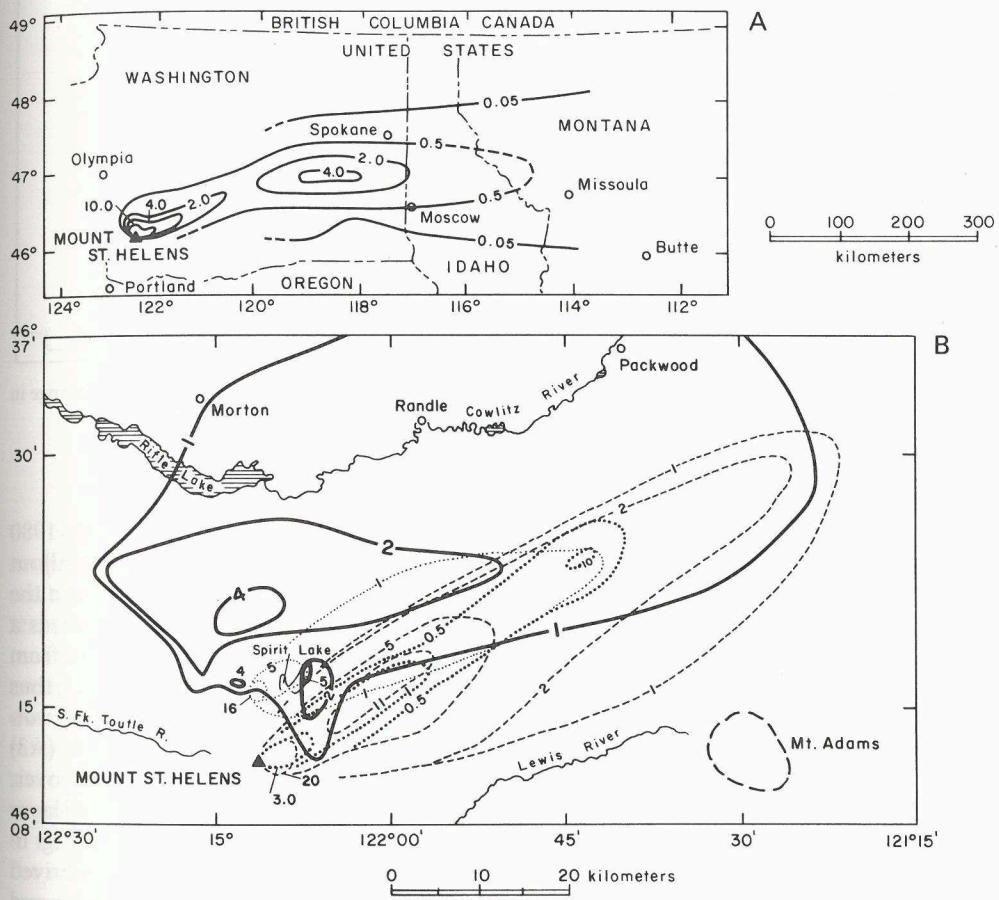


**Fig. 6-12 A, B.** Thickness distribution (in cm) of May 18, 1980 fallout ash from Mount St. Helens. **A** Distal ash, **B** proximal ash. *Solid line:* unit A; *dashed line:* unit B; *small dots:* unit C; *large dots:* unit D. See text for explanation. Contours in cm. (Sarna-Wojcicki and Shipley et al., 1981; Waitt and Dzurisin, 1981)

◀ **Fig. 6-11.** Five widespread western North American tephra layers <0.7 m.y. old. Outer limit of Mazama ash compared to area of main tephra fan illustrates difficulties in estimating volume; volume estimates of Mazama ash (Table 6-3) exclude fine-grained tephra distributed worldwide. Map is a Chamberlin Trimetric projection; major state or province boundaries, and Alaska-Canada boundary extend north-south

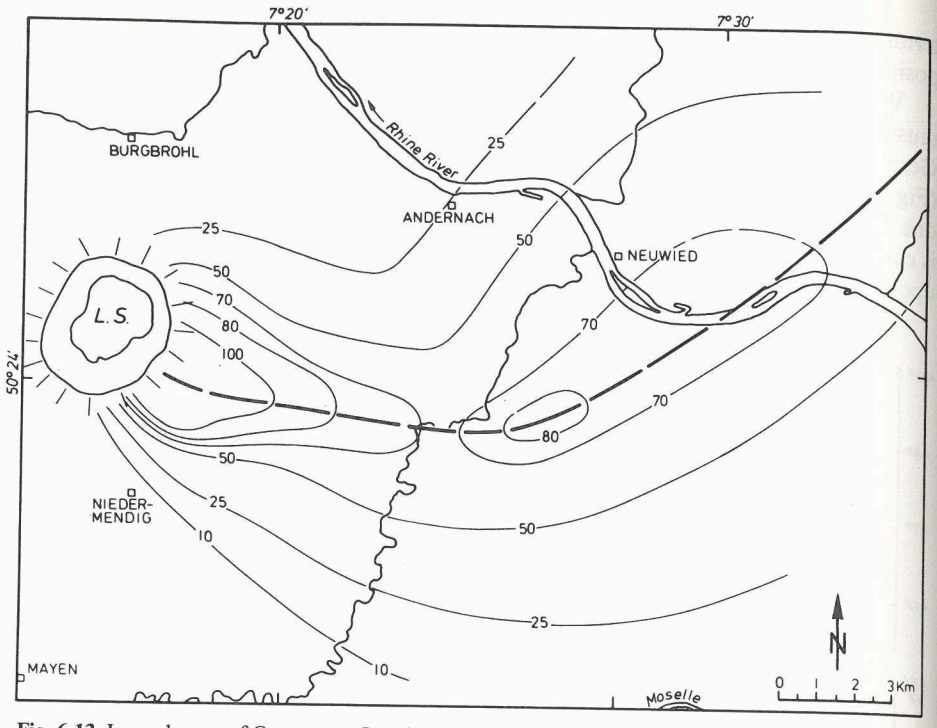


**Fig. 6-13.** Isopach map of Quaternary Laacher See fallout tephra (layer MLST C1) showing change in direction of pattern 5 km from source. Thickness in cm. (After Bogaard, 1983)

Further complexities of fallout deposition are illustrated by the May 18, 1980 eruption of Mount St. Helens, Washington. In a 12 h period, four main fallout units of different origins were deposited within a few tens of kilometers from the volcano (Fig. 6-12) (Waitt and Dzurisin, 1981). Unit A, the lowermost unit, is a basal gray lithic ash containing abundant organic material which is derived from the directed initial pyroclastic surge (terminology of Moore and Sisson, 1981), thus its thickness distribution is an irregular fan that does not have an apex at the volcano's crater. Unit A is composed of three layers, the upper one of which (A3) extends 50 km to the north and hundreds of kilometers to the northeast. Moreover, according to Waitt and Dzurisin (1981), the downwind axis of thickness of layer A3 has its apex 15 km north of the volcano within the 4-cm contour area (Fig. 6-12). Unit B, next in succession, is composed of tan, pumice, and lithic lapilli derived from vertical eruption plumes which came after the directed pyroclastic surge and shows a regular pyroclastic fan shape with its apex at the crater. Unit C is pale-brown vitric ash which has a fan-shape distribution but its apex is about 9 km north of the crater. This unit was derived from hydroclastic explosions through a hot pyroclastic flow deposit near Spirit Lake but also may in part be derived from fallout elutriated from the pyroclastic flow during its emplacement. Unit D, the uppermost and thinnest unit, is fine gray ash from the settling of fines left in the atmosphere after the events of the day, but this unit also shows a fan-shaped distribution with its apex at the crater.

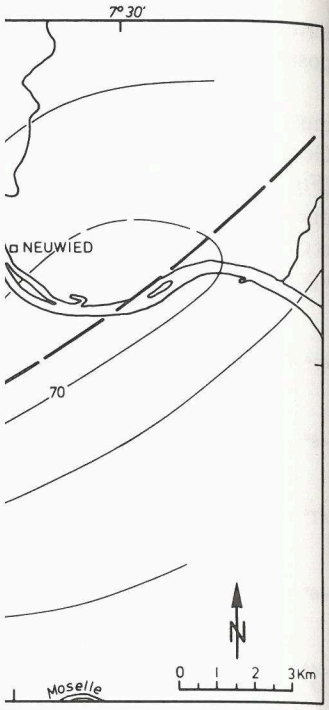


(layer MLST C1) showing change in Bogaard, 1983)

ustrated by the May 18, 1980 2 h period, four main fallout w tens of kilometers from the it A, the lowermost unit, is a aterial which is derived from Moore and Sisson, 1981), thus s not have an apex at the vol- the upper one of which (A3) rs to the northeast. Moreover, ind axis of thickness of layer he 4-cm contour area (Fig. 6- mice, and lithic lapilli derived directed pyroclastic surge and at the crater. Unit C is pale- n but its apex is about 9 km oclastic explosions through a may in part be derived from emplacement. Unit D, the up- settling of fines left in the at- shows a fan-shaped distribu-

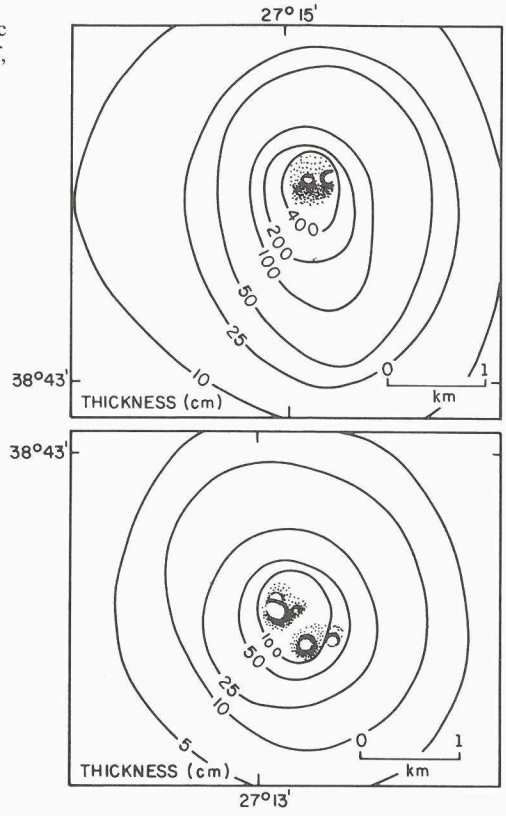


**Fig. 6-14.** Isopach maps of two small basaltic scoria cones (Terceira, Azores). (After Self, 1976)

Nearly circular isopach patterns are a common feature of low intensity basaltic eruptions (Fig. 6-14) that have low eruption columns, but individual basaltic fallout layers may be asymmetrical. Even Plinian fallout deposits may have circular patterns as at Fogo A (Azores) (Walker and Croasdale, 1971). Isopach maps may mask the existence of several eruptive events if composite sheets that form cones are not distinguished from single sheets. Cones are composed of several radiating overlapping fans within which may be a single mappable fallout unit of particular interest (Fig. 6-15). An isopach map of the cone may be a slightly elongate composite (average directions of dominant prevailing winds) of many tephra blankets. An example is the 9-year eruption of Paricutin Volcano, Mexico (Segerstrom, 1950), in which dry-season winds were generally from the east and wet-season winds from the west. Overlapping but mappable tephra fans (Fig. 6-16) from Coatepeque Volcano (El Salvador) formed the basic data used by Meyer (1972) to calculate eruptive energy (Table 6-2).

The classification scheme proposed by Walker (1973) for different eruption types (Chap. 4) relies in part upon determining the maximum thickness ($T_{max}$) of tephra sheets at their source. This is rarely measurable and therefore is commonly extrapolated graphically by assuming an exponential increase, but whether or not thickness increases exponentially is not clear. Thorarinsson (1954), for example, showed that thickness (T) is an exponential function of distance (x) from the source ($T = ae^{-kx}$; straight line on semi-log plot), but Porter (1973) shows that it is a

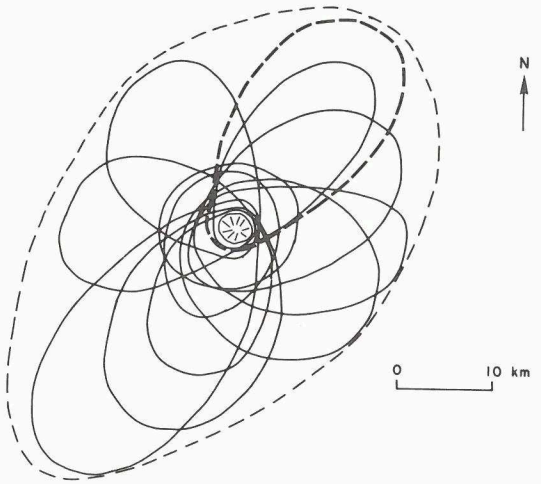


**Fig. 6-15.** Hypothetical distribution pattern of individual tephra fans distributed around a central vent. *Heavy dashed line* is a mappable fall unit. The ovate composite form of the tephra pile shown by *outer dashed line* reflects dominant annual wind direction

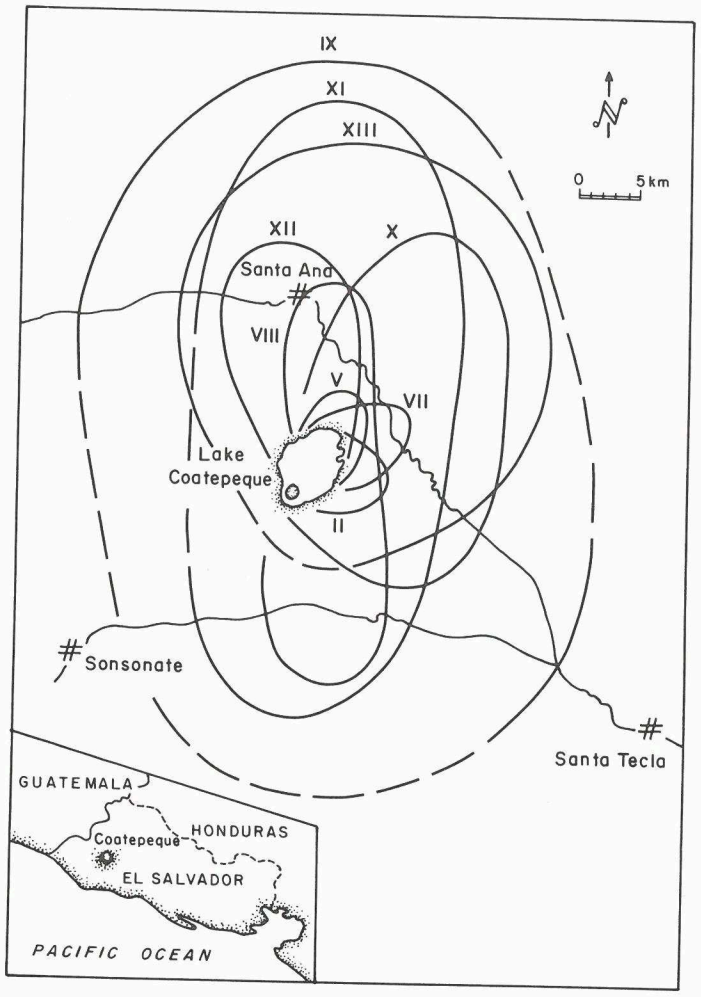


**Fig. 6-16.** Three-meter isopach lines of nine tephra layers, Coatepeque volcano (II, V, VII, VIII, IX, X, XI, XII, XIII) as designated by Meyer (1972)

**Fig. 6-15.** Hypothetical distribution pattern of individual tephra fans distributed around a central vent. *Heavy dashed line* is a mappable fall unit. The ovate composite form of the tephra pile shown by *outer dashed line* reflects dominant annual wind direction

**Fig. 6-16.** Three-meter isopach lines of nine tephra layers, Coatepeque volcano (II, V, VII, VIII, IX, X, XI, XII, XIII) as designated by Meyer (1972)

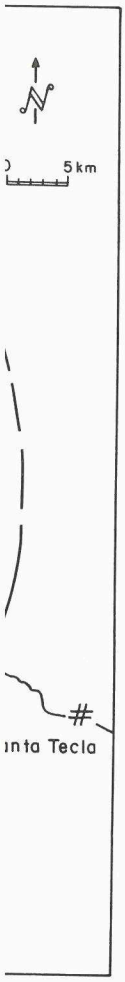


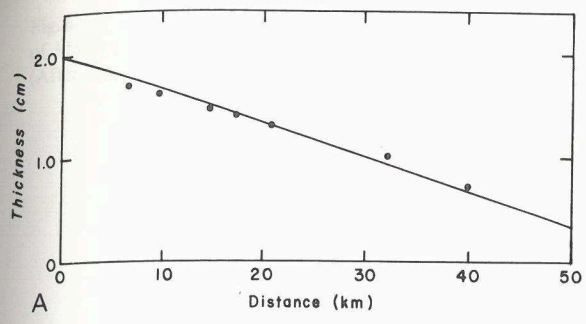


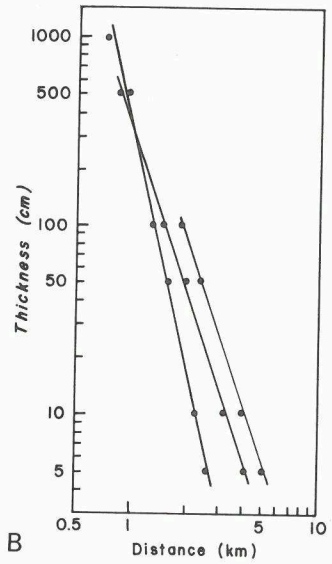


**Fig. 6-17. A** Semi-log distance/thickness plot, 1947 Hekla ash. (Thorarinsson, 1954); **B** log-log distance/thickness plot, three Holocene Hawaiian ash layers (Porter, 1973)

power function ($T = ax^{-k}$; straight line on log-log plot). The fact that Thorarinsson's (1954) data were from 2 to 40 km and Porter's (1973) from three tephra sheets 1 to 4 km from source (Fig. 6-17), suggests that the change, if it indeed exists, could be caused by a change from a dominantly ballistic transport mode to a dominantly turbulent transport mode. The thickness of Mazama ash also decreases exponentially with distance (Williams and Goles, 1968), but at about 90–100 km from source there is a marked change in slope (Fig. 6-18). Williams and Goles (1968) suggest that the tephra was carried mainly by turbulence in the eruption cloud out to about 100 km, but at greater distances it was carried by normal wind patterns. Sparks and Walker (1977), however, argue that this "fine tail" is a co-ignimbrite ashfall (Chap. 8) and not related to the Plinian fallout layer. The Laacher See, Germany, tephra layers show similar breaks in slope, the main northeast lobe at about 100 km from source and a minor southern lobe at about 10 km from source (Bogaard, 1983). At Laacher See, the volume of pyroclastic flows compared to fall-out tephra is much too small to have generated such large amounts of co-ignimbrite ash, supporting a change in dispersal mechanism proposed by Williams and Goles (1968).

## Volume

Volumes of recent and prehistoric fallout deposits (Tables 6-2 and 6-3) are easily estimated with isopach maps, but many estimates of witnessed eruptions have been made without benefit of thickness measurements and thus are suspect. Early volume estimates of the 1935 Coseguina (Nicaragua) eruption, for example, varied from 1 $km^3$ to 150 $km^3$ and were later revised to 10 $km^3$ or less (Williams, 1952). Volume data have been used to estimate volumes of magma chambers (Smith, 1979) and are used to calculate eruption energy and to construct intensity and magnitude scales of eruption (Tsuya, 1955; Yokoyama, 1957a; Hedervari, 1963; Izett,

**Table 6-2.** Area and volume of nine tephra fans within the 3-meter isopach, Coatepeque Volcano, El Salvador (Meyer, 1972)

| Area ($km^2$) | Volume ($km^3$) |
|---|---|
| 42 | 1.2 |
| 43 | 1.2 |
| 59 | 1.5 |
| 166 | 1.7 |
| 201 | 1.7 |
| 288 | 4.7 |
| 532 | 7.9 |
| 718 | 13.1 |
| 1,388 | 32.0 |

**Table 6-3.** Areal and volume estimates of tephra sheets determined from isopach maps

| Location and age | Area ($km^2$) | Volume of fallout deposits ($km^3$) | Dense-rock equivalent ($km^3$) |
|---|---|---|---|
| Nevado de Toluca volcano, Mexico | | | |
| 1. Upper Toluca Pumice, 11,600 yrs B.P. | 2,000 (within the 40 cm isopach) | 2.3 | 1.5 |
| 2. Lower Toluca Pumice, 24,500 yrs B.P. (Bloomfield et al., 1977) | 400 (within the 10 cm isopach) | 0.33 | 0.16 |
| Laacher See volcano 11,000 B.P. | | | |
| NE-Lobe | 170,000 | 12 | 3.3 |
| S -Lobe | 50,000 | 3.5 | 1.1 |
| SW-Lobe | 5,000 (within the 0.5 cm isopach) | 0.9 (?) | 0.3 (?) |
| (Bogaard, 1983) | | | |
| Mount Mazama, Oregon, 6,600 yrs B.P. (Williams and Goles, 1968, Fryxell, 1965) | 900,000 | 29–37 | |
| White River Ash, Yukon Territory | | | |
| North Lobe, 1887 yrs B.P. | ~320,000 | 25 | |
| East Lobe, 1250 yrs B.P. (Lerbekmo et al., 1975) | | | |
| Pompeii, Italy, 79 A.D. (Lirer et al., 1973) | | 2.6 (est.) (only 0.80 deposited on land) | 0.53 |
| Santa Maria, Guatemala, 1902 (Sapper, 1904, Rose, 1972) | 150 (within the 1 m isopach) | 5.5 | |
| Hekla, Iceland, 1947 (Thorarinsson, 1954) | (3,130 on land) 70,000 total (within 0.006 cm isopach) | 0.18 | 0.045 |

ed from isopach maps

| olume of fallout :posits $m^3$) | Dense-rock equivalent ($km^3$) |
|---|---|
| :.3 | 1.5 |
| ).33 | 0.16 |
| | 3.3 |
| .5 | 1.1 |
| .9 (?) | 0.3 (?) |
| -37 | |
| 5 (est.) (only 0.80 deposited on land) | 0.53 |
| 5 | |
| 18 | 0.045 |

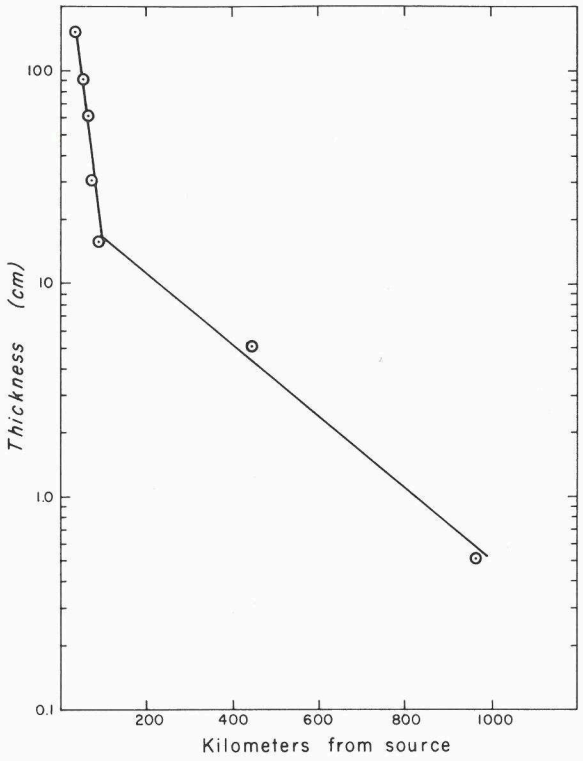


**Fig. 6-18.** Variations in thickness of Mazama tephra with distance. (After Williams and Goles, 1968)

1981). The values have been generally underestimated, however, because the amount of finer-grained material transported great distances can exceed the volume of the mappable fan deposit (Williams and Goles, 1968) (Fig. 6-11). To determine the volume of the Taupo pumice, New Zealand, and several other Plinian deposits, Walker (1980) plots the area enclosed by isopachs on a log-log area-thickness graph (Fig. 6-19); volume is then determined from the area beneath the resulting curves. This and other methods for determining volume are discussed by Froggatt (1982).

Several workers have drawn attention to the similarity between fallout patterns of tephra and other types of material, notably radioactive aerosol particles, and have developed theoretical models to account for the distribution patterns of both types of components (Knox and Short, 1963; Slaughter and Hamil, 1970; Scheidegger and Potter, 1968; Eaton, 1964; Shaw et al., 1974).

## Structures

### Bedding

In general, bedding in near-source fallout deposits consists of alternating gradational coarse-grained to finer-grained layers without sharp bedding planes (Fig. 6-20), but whether bedding is sharp or gradational depends upon several factors. These are: (1) the duration and energy fluctuations of an eruption; (2) vol-

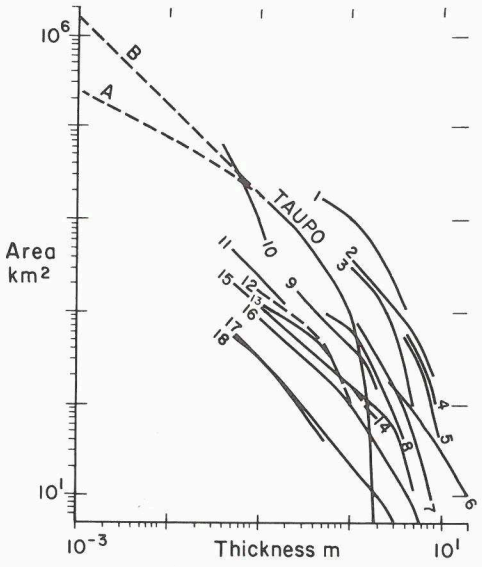


**Fig. 6-19.** Plot of area enclosed by isopachs vs. thickness for Taupo pumice, New Zealand and other Plinian pumice deposits: *1* Ontake (Kobayashi et al., 1967), *2* Shikotsu (Katsui, 1959), *3* Askja 1875 (G. P. L. Walker, unpublished data), *4* Tenerife J (Booth and Walker, unpublished), *5* Granadilla (Booth, 1973), *6* Pompeii (Lirer et al., 1973), *7* La Primavera B (Clough, Wright, and Walker, unpublished), *8* Toluca upper member (Bloomfield et al. 1977), *9* Fogo 1563 (Walker and Croasdale, 1971), *10* Fogo A (Walker and Croasdale, 1971), *11* Crater Lake (Fisher, 1964b), *12* Hekla 1947 (Thorarinsson, 1954), *13* Tenerife L (Booth and Walker, unpublished), *14* Mangaone (Howorth, 1975), *15* La Primavera J (Clough et al., in Walker 1980), *16* Hekla H3 (Thorarinsson, 1967b), *17* Furnas C (Booth et al., 1978), *18* Avellino (Lirer et al., 1973). (After Walker, 1980)

ume and discharge rate of tephra; (3) direction and strength of winds during an eruption; and (4) the length of time between eruptions during which erosion, weathering or winnowing of the depositional surface may take place (Fig. 6-21, 6-22). Moreover, a change in composition of material being erupted may result in the deposition of two or more layers that have narrow gradational boundaries (Thorarinsson, 1954; Waitt and Dzurisin, 1981; Bogaard, 1983).

Individual beds of fallout tephra commonly have few or no internal structures or laminations. They are set apart from one another by color differences caused by different compositions (or varying percentages of different juvenile fragments) and by post-depositional diagenetic changes, by sorting, or by grain size or grading differences (Mullineaux, 1974; Waitt and Dzurisin, 1981). A continuous, voluminous, and irregularly pulsating eruption of high intensity (Plinian) lasting several hours or days may deposit sequences composed of numerous alternating and gradational coarse- to fine-grained beds with a combined thickness of many meters (Fig. 6-23). Such an eruption, however, may also produce a continuous rain of fragments of different sizes deposited together and at random, resulting in a single, thick, poorly sorted layer without distinct internal laminae. Walker (1980) relates such beds to fluctuating discharge rates, column height and therefore particle fall velocities as shown in Fig. 6-24).

Material suspended by wind currents is deposited as thin tephra blankets over long distances, as witnessed during the May 18, 1980 eruption of Mount St. Helens, Washington (Sarna-Wojcicki and Shipley et al., 1981). Such thin deposits, if preserved, commonly lack internal bedding. Farther from source, later and earlier eruption fragments in the eruption cloud may even become mixed (Salmi, 1948). Areas receiving periodic light ash falls from distant volcanoes may gradually build up thick homogeneous ash deposits lacking bedding (caused by bioturbation and other soil-forming processes) that resemble wind-blown dust (loess) in nearly every aspect (Taylor, 1933; Fisher, 1966d) (Fig. 6-25).

ig. 6-19. Plot of area enclosed by isopachs vs. ıickness for Taupo pumice, New Zealand ıd other Plinian pumice deposits: *1* Ontake obayashi et al., 1967), *2* Shikotsu (Katsui, 959), *3* Askja 1875 (G. P. L. Walker, unpub-shed data), *4* Tenerife J (Booth and Walker, ıpublished), *5* Granadilla (Booth, 1973), *6* ompeii (Lirer et al., 1973), *7* La Primavera B lough, Wright, and Walker, unpublished), Toluca upper member (Bloomfield et al. 977), *9* Fogo 1563 (Walker and Croasdale, 971), *10* Fogo A (Walker and Croasdale, 971), *11* Crater Lake (Fisher, 1964b), *12* ekla 1947 (Thorarinsson, 1954), *13* Tenerife (Booth and Walker, unpublished), *14* langaone (Howworth, 1975), *15* La Primavera (Clough et al., in Walker 1980), *16* Hekla H3 horarinsson, 1967b), *17* Furnas C (Booth al., 1978), *18* Avellino (Lirer et al., 1973). ıfter Walker, 1980)

ı and strength of winds during an eruptions during which erosion, ırface may take place (Fig. 6-21, 6- ıterial being erupted may result in ve narrow gradational boundaries Bogaard,1983).

have few or no internal structures nother by color differences caused ges of different juvenile fragments) sorting, or by grain size or grading isin, 1981). A continuous, volumi- h intensity (Plinian) lasting several sed of numerous alternating and ombined thickness of many meters lso produce a continuous rain of nd at random, resulting in a single, nal laminae. Walker (1980) relates n height and therefore particle fall

osited as thin tephra blankets over 1980 eruption of Mount St. Helens, , 1981). Such thin deposits, if pre- her from source, later and earlier even become mixed (Salmi, 1948). ant volcanoes may gradually build ılding (caused by bioturbation and l-blown dust (loess) in nearly every

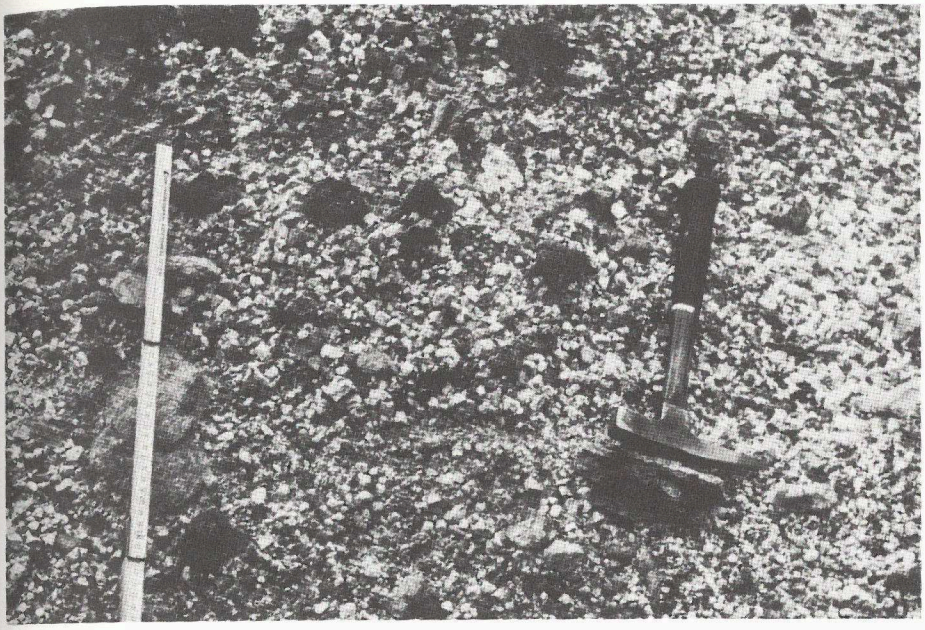

**Fig. 6-20.** Near-vent fallout deposits consisting of pumice lapilli and abundant basanite and sandstone blocks. Note angularity of pumice lapilli and scarcity of fine-grained matrix. About 1 km from vent, Laacher See tephra (Eifel, Germany)

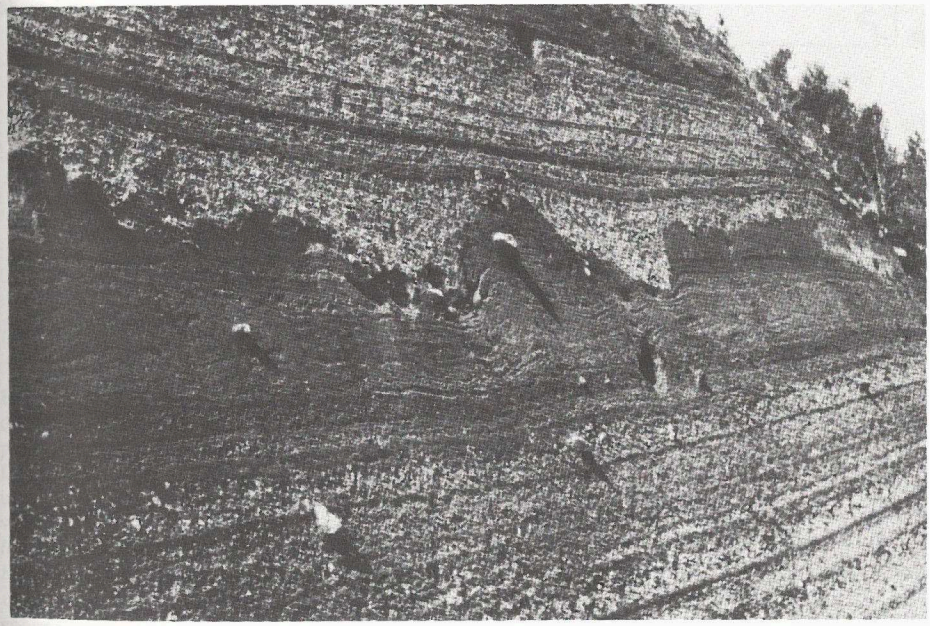

**Fig. 6-21.** Erosional unconformity between two cycles of late Quaternary trachytic eruptions dominated by coarse Plinian fallout in the lower and fine-grained, in part massive, accretionary lapilli-bearing surge and fallout in the upper part. Rim of Sete Cidades Caldera (São Miguel, Azores)

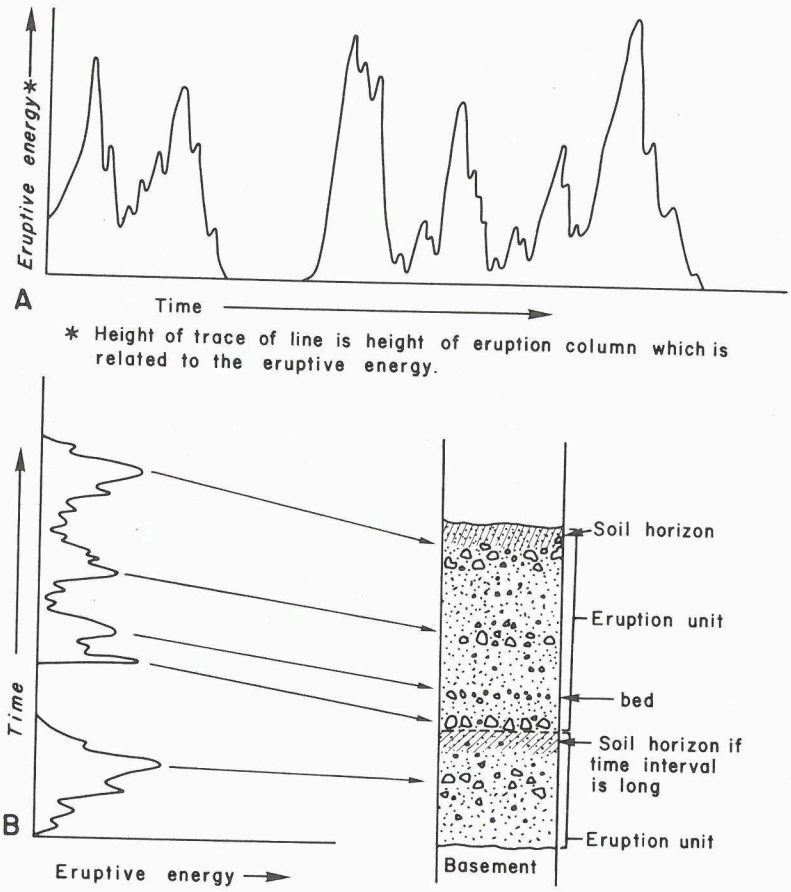


**Fig. 6-22 A, B.** Hypothetical correlation of eruption diagram energy peaks, **A** with bedded sequence, **B** of pyroclastic rocks. Other factors that affect bedding are wind direction and velocity, characteristics of eruption column and distance to source (presence or absence of ballistic fragments). Development of bedding also depends upon pulse time of eruption column versus fall time of fragments

## Mantle Bedding

Fallout tephra commonly mantles all but slopes greater than about 25–30 degrees, a feature that has long been recognized as characteristic of fallout tephra (Wentworth, 1938). Tephra drapes over hills and valleys, into small depressions and channels, and over any other roughness elements of the landscape (Figs. 6-23 to 6-27). Wind, water, and gravity immediately begin the downhill transfer of material into low areas, but rapidly buried ash may retain high initial dips. The rate of downhill transfer depends upon (1) the transporting agent, (2) the size and shape of fragments, (3) angle of slope, (4) rate of deposition, (5) amount and type of vegetation and (6) climate (humid versus arid, etc.). Sheet flooding or rill development is inhibited in freshly deposited, coarse-grained, highly permeable tephra, but in fine-grained deposits light rain causes relatively hard crusts to develop on fresh ash;

umn which is

Soil horizon

Eruption unit

— bed

- Soil horizon if time interval is long

Eruption unit

gy peaks, **A** with bedded sequence, **B** direction and velocity, characteristics of ballistic fragments). Development s fall time of fragments

ater than about 25–30 degrees, ristic of fallout tephra (Went- s, into small depressions and of the landscape (Figs. 6-23 to the downhill transfer of mate- n high initial dips. The rate of g agent, (2) the size and shape n, (5) amount and type of veg- et flooding or rill development ghly permeable tephra, but in crusts to develop on fresh ash;

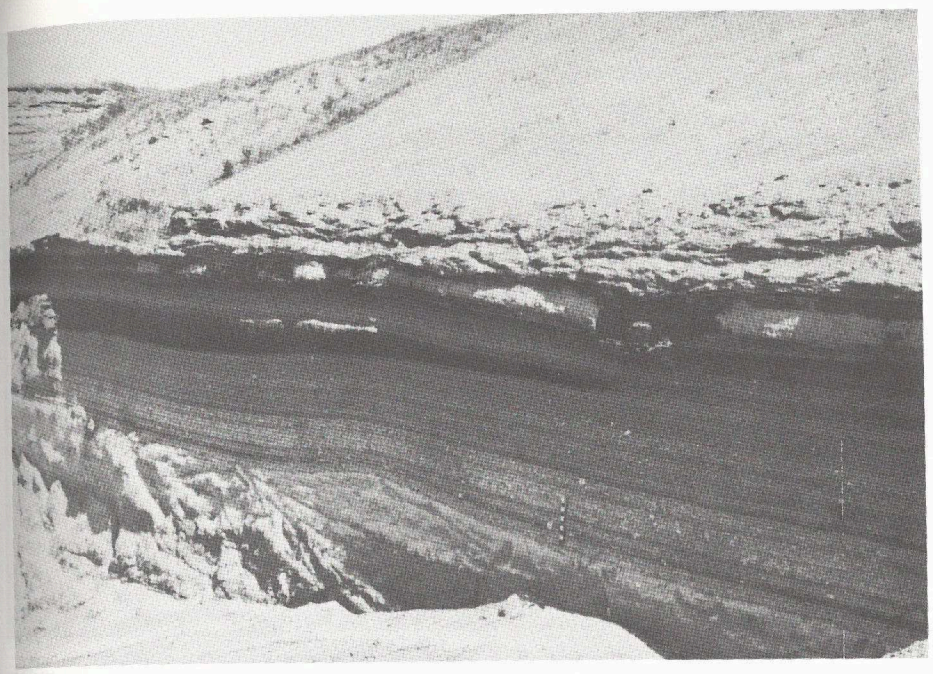

**Fig. 6-23.** Lateral termination of pyroclastic flow deposit interbedded with Plinian pumice lapilli layers. Note mantle bedding where fallout tephra layers overlie basal light-colored pyroclastic flow deposit. Bedding in fallout sequence is due to differences in grain size, thin ash cloud layers and change in composition, the deposit becoming darker and more mafic upwards. Laacher See tephra (Eifel, Germany), about 5 km from source. Scale in 10-cm intervals

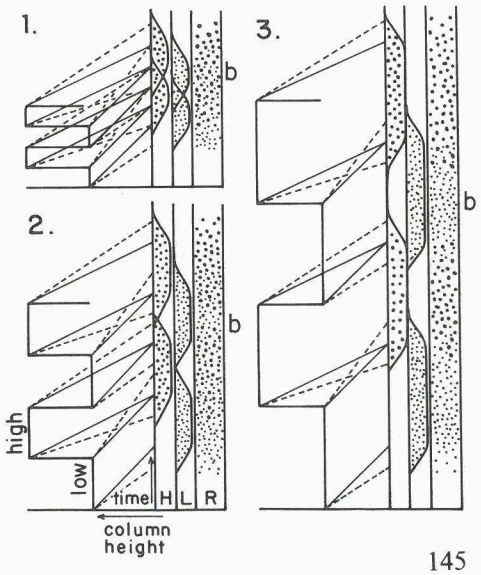


**Fig. 6-24.** Diagrammatic representation of the development of gradational bedding from a pulsating eruption column. *H* deposition from high column; *L* deposition from low column; *R* resultant. *Dashed line* is a standard deviation in fall time equal to one-third to the fall time. *1* column pulsations are shorter than fall time; deposition from second low column does not produce a discrete bed at *b*. *2* column pulse time is comparable to fall time; discrete bed beginning to appear at *b*. *3* column pulse time is longer than fall time; well-defined bed at *b*. (After Walker, 1980)

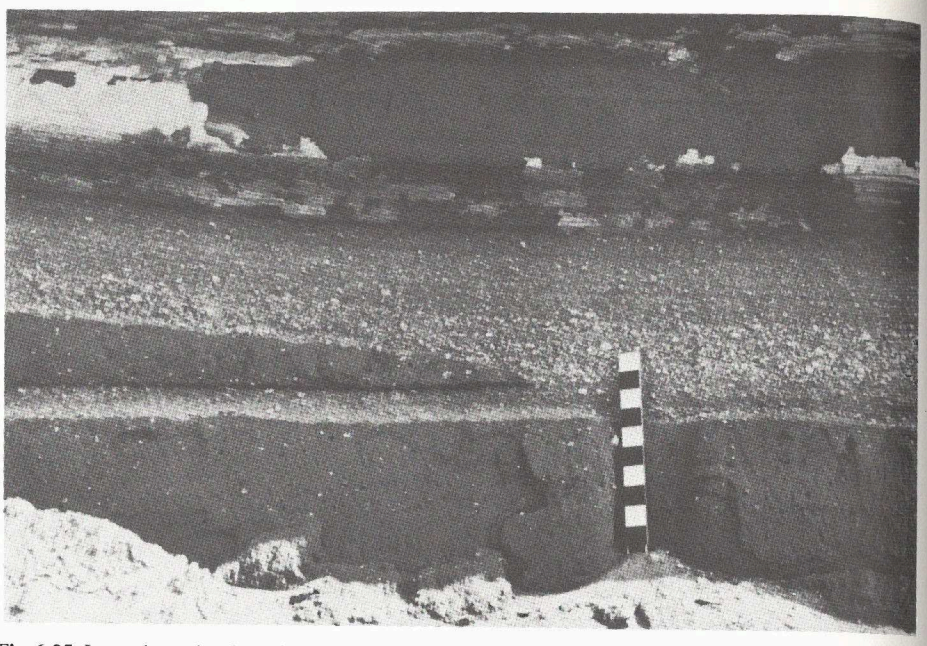

**Fig. 6-25.** Lateral termination of pyroclastic flow deposit showing flat base and curved top interbedded with pumice lapilli and lower pyroclastic flow deposit. Quaternary Laacher See tephra (Eifel, Germany). Fine-grained bedded surge and massive fallout tephra at top represent terminal phase of eruption. Scale in 10-cm intervals

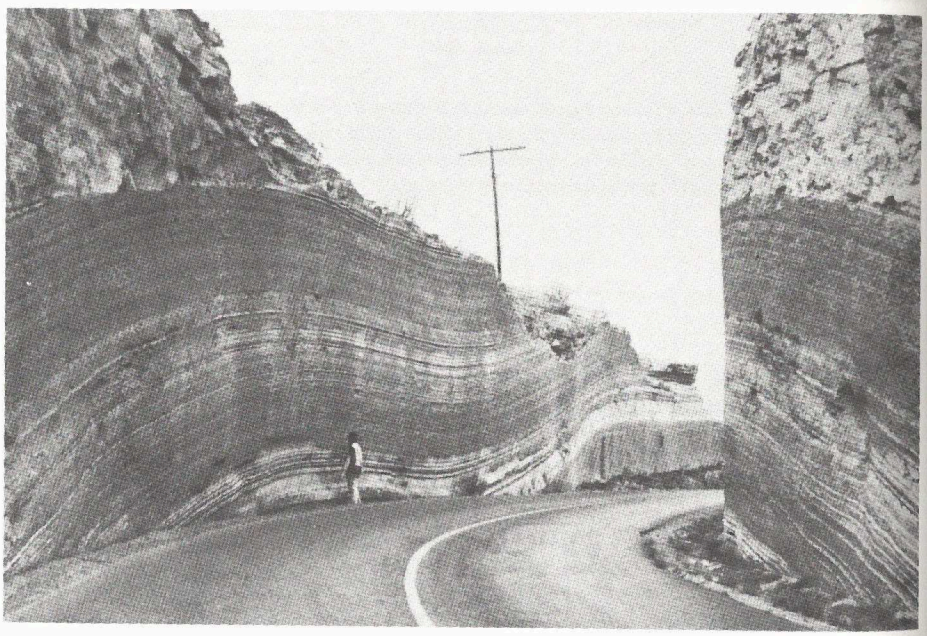

**Fig. 6-26.** Mantle bedding of late Quaternary trachytic fallout tephra overlying basaltic lava flow (end of road cut). Tenerife (Canary Islands)

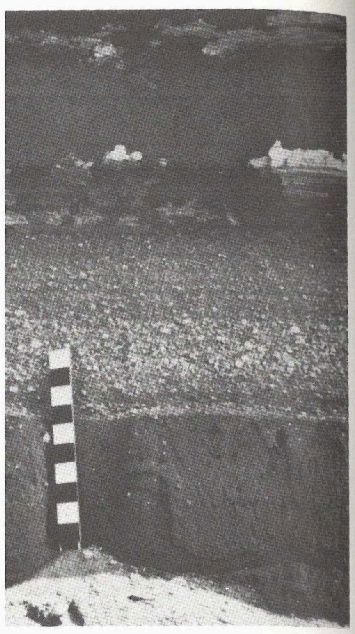

g flat base and curved top interbedded
nary Laacher See tephra (Eifel, Ger-
top represent terminal phase of erup-

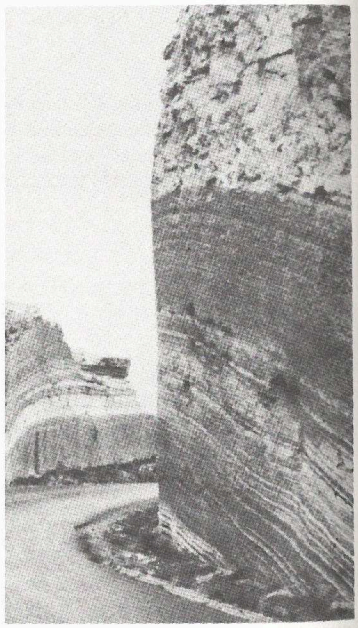

ephra overlying basaltic lava flow (end

this lessens permeability and accelerates erosional processes (Fig. 6-22) (Segerstrom, 1950; Waldron, 1967). Thick ash deposits at Paricutin Volcano, Mexico, disrupted or destroyed the original drainage pattern and killed vegetation. With changes in slope caused by growth of the volcano, erosion was accelerated and new streams quickly cut to levels below the old stream-bed levels.

Fragments falling directly from above roll, slide or avalanche down steep-sided channels to deposit wedge-shaped layers in cross-section (Fig. 6-27). Depending upon channel width, these deposits may be thicker inside than outside the channel. With equal volumes, individual layers progressively decrease in thickness upward as the cross sectional area of the channel increases. Over undulating topography, layers thicken and thin depending upon slope angles and trajectory of the path of the falling particles.

Broad-scale topographic smoothing caused by long-term ($\sim$5 million years) deposition and reworking of pyroclastic debris is well illustrated by the Oligocene-Miocene John Day Formation of central Oregon (Fisher, 1964a). The lowermost member covers ancient hills with slopes of up to 25 or 30 degrees; in low areas, the ash accumulated in lakes and marshes. Later members filled broad, gentle valleys several kilometers wide; they thin toward broad structural highs. The changes in thickness occur over such broad areas that they are only revealed by detailed mapping of facies and measured sections (Fisher, 1967; Fisher and Rensberger, 1973).

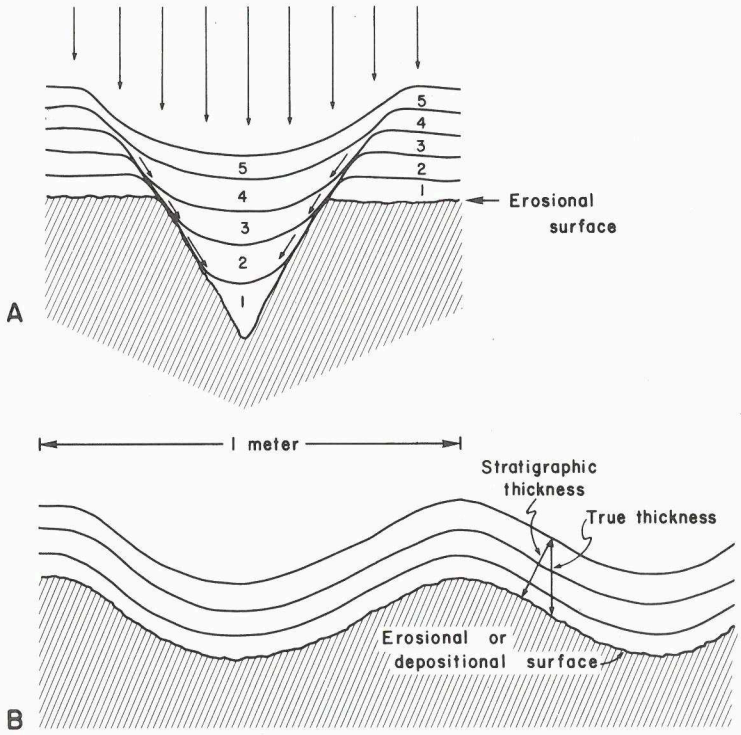


**Fig. 6-27 A, B.** Idealized diagram showing influence of relatively small-scale topographic irregularities on shape and thickness of fallout layers

In some places high initial dips on pre-existing hilly topography might be mistaken for tectonic deformation.

### Graded Bedding

It is expected that particles falling out of the atmosphere would form density- or size-graded layers with the largest and heaviest particles at the base, but several factors work against perfect grading. These include fluctuations in eruption energy, wind direction and strength, turbulence in the eruption column, and rain flushing. As distance from the volcano increases and particle transport is by wind rather than by fluctuations in eruption energy, settling velocity becomes a more important factor and therefore normal grading becomes increasingly common.

Normal and reverse grading in Plinian and sub-Plinian pumice deposits has been described by Booth (1973), Lirer et al.(1973), Self (1976), and Bloomfield et al.(1977) (Fig. 6-28). Possible causes listed by Self (1976) for reverse grading are: (1) A progressive increase in initial gas velocity during the eruption ejects larger fragments to greater heights in the later phases, promoting a wider dispersal by the wind (Lirer et al., 1973; Booth, 1973); (2) A change in vent morphology from cylindrical to conical as the eruption proceeds enables particles to be ejected at lower angles and therefore to travel farther (Murata et al., 1966). This effect is observed only very near the vent; (3) For a constant gas velocity, an increase in eruption column density by an increase in the percentage of very fine dust in the eruption column can increase the release height of individual large clasts from the column and therefore the range of dispersal of large clasts (Wilson, 1976); (4) Widening of the conduit radius as the eruption proceeds may reduce the frictional drag acting on the high velocity flow of gas and particles, thereby giving an increased exit velocity if the same mean gas velocity is maintained. An additional cause is erratic changes in wind velocity and direction during eruption.

Slope instability at the time of deposition also effects grading. Reverse-graded pumice beds of the Coso Range, California are attributed to rapid accumulation of pumice during eruption on steep surfaces causing downslope grain flows (Duffield et al., 1979). Reverse grading develops from grain-dispersal pressures where larger grains move (upward) toward the zone of least shear strain within a grain flow (Bagnold, 1954b) such as occurs in avalanche deposits on the slip face of sand dunes (Bagnold, 1954a). Reverse-graded beds also develop by dry grain flows on cinder cones where slopes attain steep angles (Wentworth and Macdonald, 1953) (Figs. 6-29, 6-30) and by frost-heaving in cold climates.

## Fabric

Particle orientation in fallout tephra is commonly isotropic, but anisotropic fabric may occur if particles are elongate or platy. Close to the eruptive source, however, rapidly deposited large and small fragments may remain supported at various angles in a crowd of neighboring particles (Fig. 6-20). At long distances, elongate or platy particles falling from suspension tend to land parallel to depositional surfaces.

ɔpography might be mistaken

ɔhere would form density- or
ticles at the base, but several
fluctuations in eruption ener-
ption column, and rain flush-
cle transport is by wind rather
ɔcity becomes a more impor-
reasingly common.
-Plinian pumice deposits has
elf (1976), and Bloomfield et
976) for reverse grading are:
ing the eruption ejects larger
oting a wider dispersal by the
in vent morphology from cy-
ɔarticles to be ejected at lower
1966). This effect is observed
y, an increase in eruption col-
fine dust in the eruption col-
ge clasts from the column and
ɔn, 1976); (4) Widening of the
the frictional drag acting on
ving an increased exit velocity
tional cause is erratic changes

ects grading. Reverse-graded
ibuted to rapid accumulation
downslope grain flows (Duf-
ain-dispersal pressures where
st shear strain within a grain
posits on the slip face of sand
levelop by dry grain flows on
worth and Macdonald, 1953)
s.

ɔtropic, but anisotropic fabric
the eruptive source, however,
remain supported at various
). At long distances, elongate
d parallel to depositional sur-

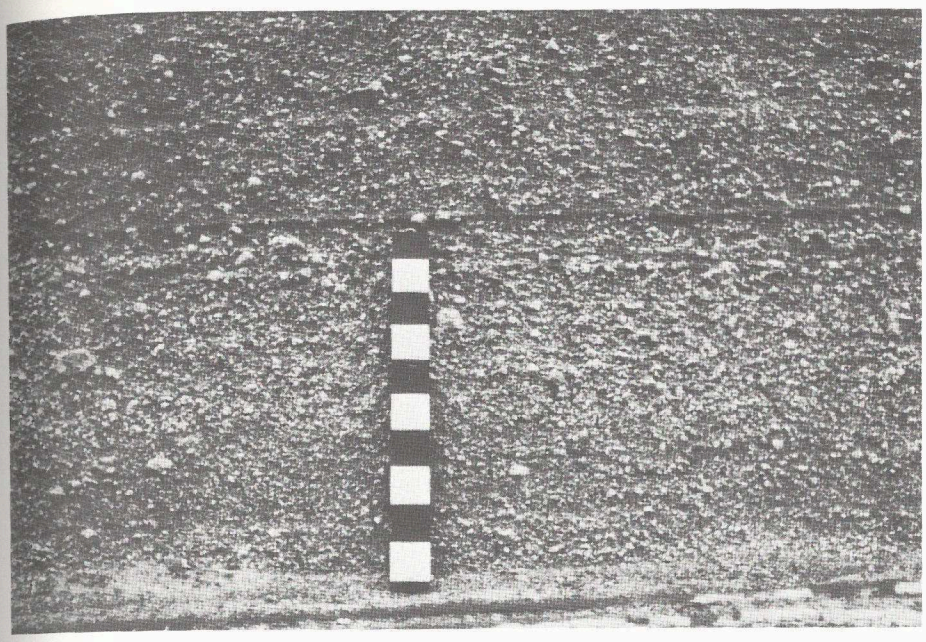

**Fig. 6-28.** Reverse grading in one meter thick phonolitic Plinian fallout tephra overlain by darker more mafic fallout and pyroclastic flow deposit. Scale in 10-cm intervals. Laacher See (Eifel, Germany)

**Fig. 6-29.** Inversely graded deposits of basaltic composite lapilli. Quaternary Herchenberg volcano (Eifel, Germany)

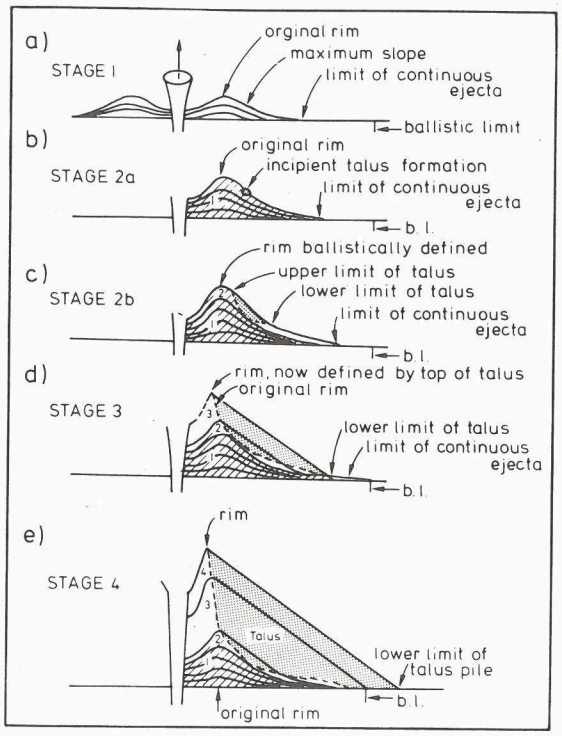


**Fig. 6-30 a–e.** Development of cinder cones in four stages. **a** Stage 1, low rimmed scoria and tuff ring. **b, c** Stage 2, build-up of rim and development of exterior talus. **d** Stage 3, slumping and blast erosion causes destruction of original rim. **e** Stage 4, talus extends beyond ballistic limit of ejecta as volume of cone grows. (After McGetchin et al., 1974)

## Size Parameters

Although structural aspects are most useful for identifying fallout layers in the field, textural parameters determined by laboratory granulometric analysis provide information about eruption mechanics, vent location, height of eruption column, energy of eruption, wind conditions, etc. when used in conjunction with isopach maps. Parameters most commonly used are maximum size of components, median diameter and sorting values.

### Maximum Size of Components

The maximum diameters of lithic and pumice fragments in fallout deposits have been measured to infer vent location, relative volcanic energy, inclination of eruption column, and wind directions (Minakami, 1942; Kuno et al., 1964; Fisher, 1964b; Walker, 1971; Walker and Croasdale, 1971; Suzuki et al., 1963; Lirer et al., 1973; Self, 1976; Schmincke, 1977 b; Bloomfield et al., 1977; Booth et al., 1978; Walker, 1980; Bogaard, 1983). The maximum diameter of a selected number of the largest pumice and lithic fragments is measured in the field; the arithmetic mean of each set of measurements may be then plotted graphically or as isograde maps. The number of fragments measured per outcrop varies from 10 (e.g. Kuno et al., 1964) to 5 (e.g. Minakami, 1942) to as few as 3 (e.g. Walker and Croasdale, 1971). All studies show an exponential decrease in maximum diameter of both types of

**Fig. 6-30 a–e.** Development of cinder cones in four stages. **a** Stage 1, low rimmed scoria and tuff ring. **b, c** Stage 2, build-up of rim and development of exterior talus. **d** Stage 3, slumping and blast erosion causes destruction of original rim. **e** Stage 4, talus extends beyond ballistic limit of ejecta as volume of cone grows. (After McGetchin et al., 1974)

**Fig. 6-31 a, b.** Average maximum diameter of pumice fragments (**a**) and lithic fragments (**b**) vs. distance from vent for Fogo A (Azores) pumice sheet. (After Walker and Croasdale, 1971)

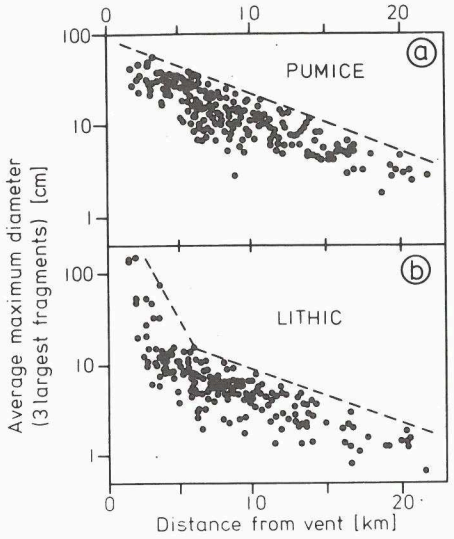


components away from the source (Fig. 6-31). Some authors note that maximum lithic fragment sizes decrease sharply in the first 2 km or so and then more gradually away from the source. This is attributed to ballistic transport of the largest lithic fragments near the source (Walker and Croasdale, 1971; Self, 1976; Schmincke, 1977 b; Booth et al., 1978) (Fig. 6-32). The maximum size of lithic fragments is commonly about half that of pumice in the same outcrop depending on their relative densities. Equidimensional lithic fragments give more consistent results than platy components because factors influencing settling velocity of platy fragments are more complex. Brittle pumice can break upon impact (Fig. 5-2), and, if not recognized, this can lead to significant errors. Distribution patterns of isograde maps that differ from isopach maps of the same deposit near the source may be attributed to directional wind patterns at different altitudes (Fisher, 1964b; Waitt and Dzurisin, 1981) or to inclined eruption columns (Fig. 6-33).

### Median Diameter

Median diameters of material within pyroclastic layers exponentially decrease overall away from the source but in detail the decrease is rarely systematic. Median diameters may provide a more sensitive indicator of inclined eruptions or wind variations during an eruption than do isopach maps alone (Fisher, 1964b; Walker, 1980) but require more laboratory time to determine than field measurement of maximum diameters. Also, the sampling from thick tephra layers with vertical variations in size parameters (Fig. 6-34) may introduce large errors, and because tephra layers are polycomponent, further complications may occur. The relationship between median diameter, distance to source and relative amounts of crystals-lithics-pumice is given by Walker and Croasdale (1971) and Booth et al., 1978 (Fig. 6-35). A general median diameter-distance plot for polycomponent tephra samples (Fig. 6-36) is useful to infer broad limits for travel distance where the source is un-

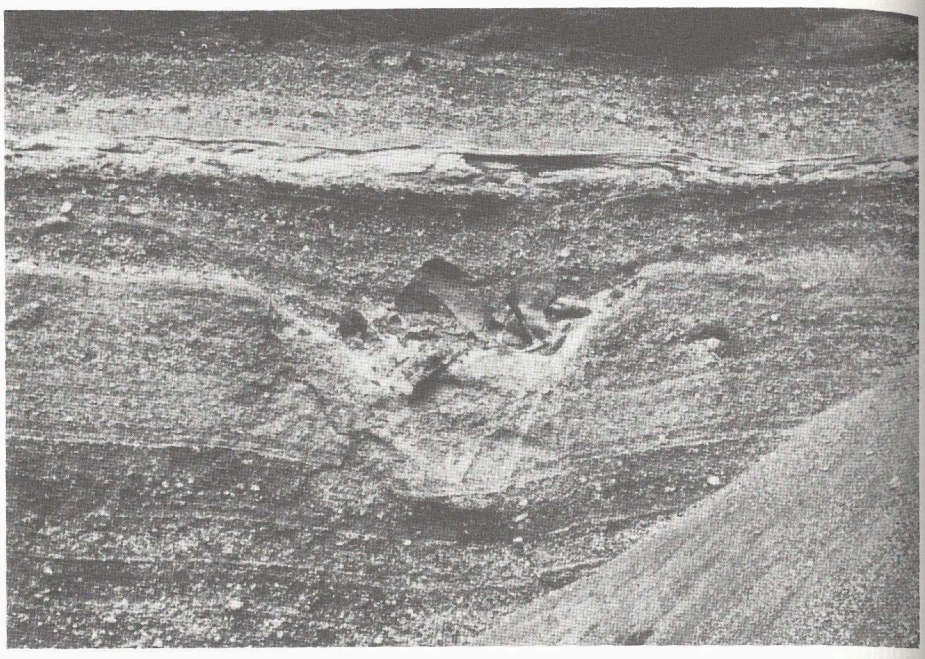

**Fig. 6-32.** Basalt block emplaced ballistically into pumice lapilli layers. Zone of compacted and faulted lapilli extends for about 1 m beneath block. Late Quaternary Laacher See tephra (Eifel, Germany)

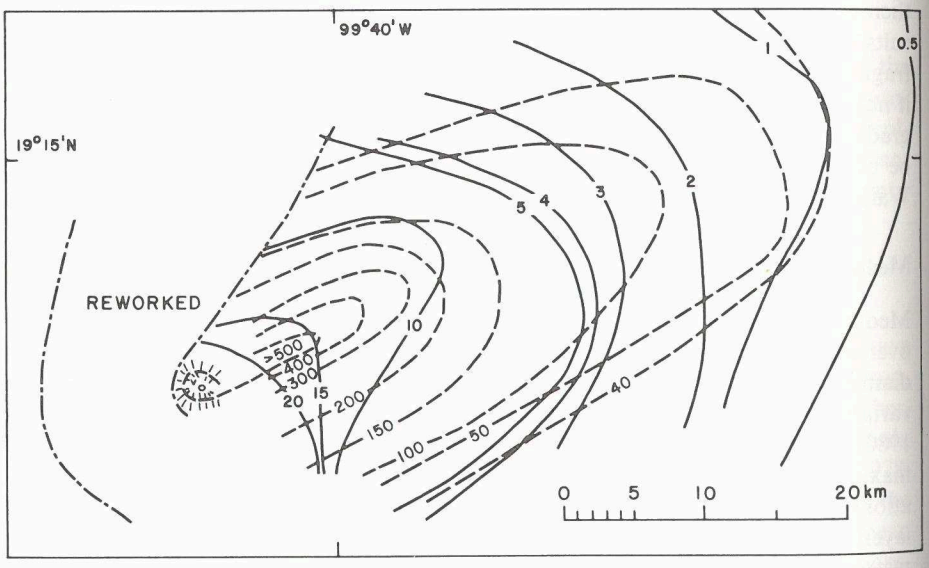


**Fig. 6-33.** Isopach map (*dashed line*) of Upper Toluca Pumice (thickness in cm), Nevado de Toluca Volcano, Mexico, upon which are superimposed contours (in cm) of average maximum diameter of the five largest pumice fragments from Lower Member (*solid lines*). Illustrates different axes of distribution. Vent is *hachured*. (After Bloomfield et al., 1977)

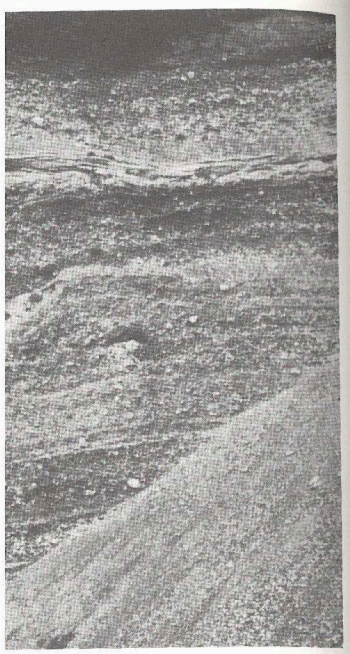

ayers. Zone of compacted and faulted
cher See tephra (Eifel, Germany)

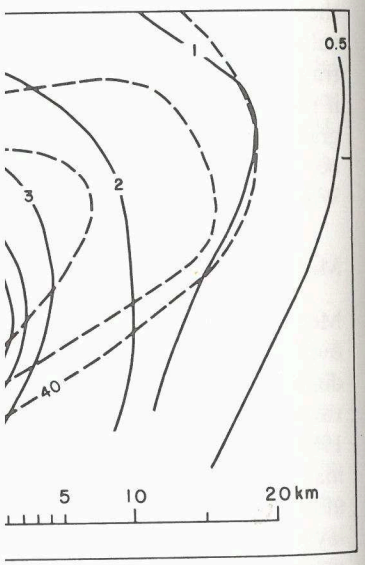


nickness in cm), Nevado de Toluca Vol-
f average maximum diameter of the five
lustrates different axes of distribution.

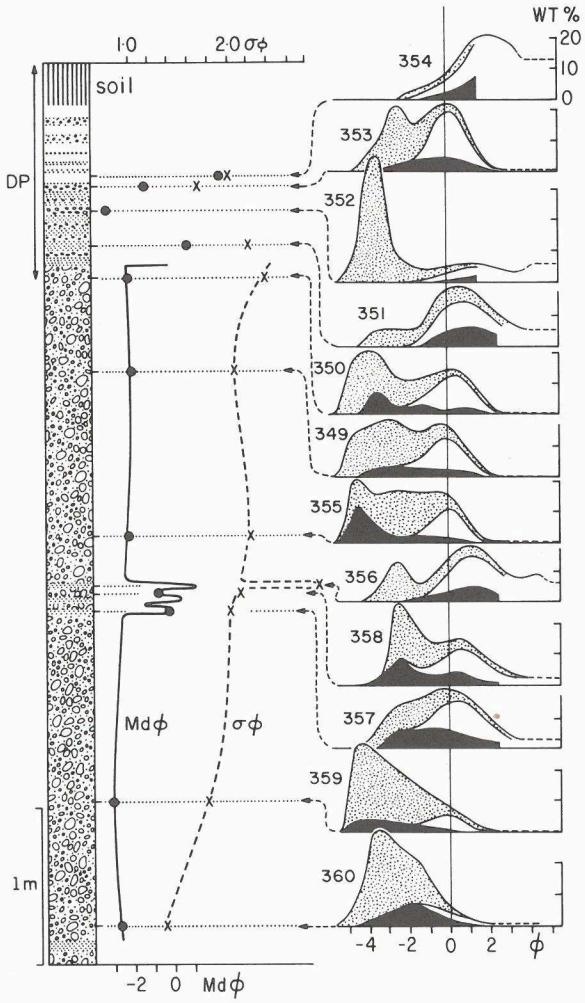


**Fig. 6-34.** Median size ($Md_\phi$), Inman sorting coefficient ($\sigma_\phi$) and frequency distribution of pumice (*stippled*), crystals (*unornamented*) and lithics (*solid*) for Fogo A tephra, 3.7 km southeast of Lake Fogo (São Miguel, Azores). (After Walker and Croasdale, 1971)

known, but cannot be used to determine exact limits because of wide scatter. For example, fallout tephra with $Md_\phi = -3.0$ (8 mm) is probably within 60 km or less of its source.

### Grain-Size Distribution (Sorting)

In general, good sorting is an important criterion for distinguishing fallout ash from pyroclastic flow deposits (Walker, 1971). For example, fine-grained dust is less abundant in coarse-grained pumiceous fallout layers than in nonwelded pyroclastic flow deposits. Sorting coefficients ($\sigma_\phi$, Inman, 1952) determined granulometrically for many samples have been published by Murai (1961), Fisher (1964b), Walker and Croasdale (1971), Walker (1971; 1980), Sheridan (1971), Kittleman (1973), Lirer et al., (1973), Schmincke (1977 b), Self (1976) and Booth et al., (1978).

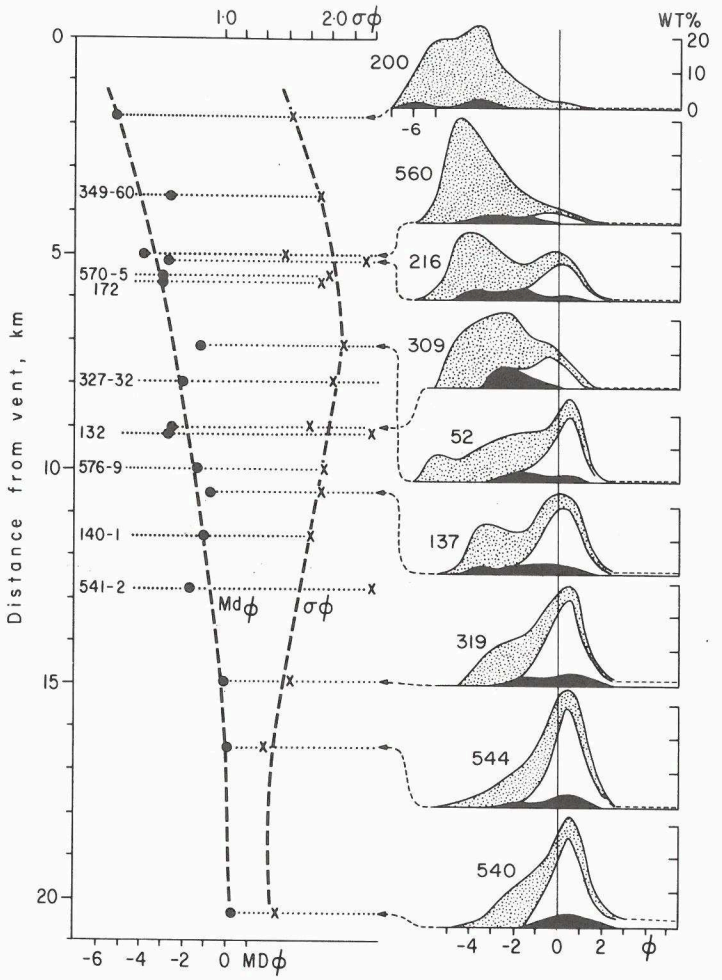


**Fig. 6-35.** Lateral changes from Lake Fogo (Azores) in median diameter ($Md_\phi$), Inman sorting coefficient ($\sigma_\phi$) and frequency curves for pumice (*stippled*), crystals (unornamented) and lithics (*solid*) for nine samples, Fogo A pumice deposit. (After Walker and Croasdale, 1971)

From the summaries of Fisher (1964b) and Walker (1971), it appears that most fallout tephra deposits have sorting values between 1 and 2, with most around 1.4. Overall, sorting becomes better with increasing distance from the vent (Fisher, 1964b) but the pattern is complex in detail. For example, small-particle agglutination to form accretionary lapilli can cause sedimentation of fine-grained material alongside coarse material (Carey and Sigurdsson, 1982). And, at small distances from the vent (about 30 km, depending on grain size), sorting values may increase prior to a decrease (Walker, 1971; Walker and Croasdale, 1971; Suzuki et al., 1973; Schmincke, 1977 b). Much of this variation at a few kilometers from the vent is due to pronounced differences in density between pumice, crystals, and rock fragments. Thus, in tephra deposits on Fogo, Azores (Walker and Croasdale, 1971) the grain size distribution is unimodal (mode $-3_\phi$ to $-4_\phi$) and positively skewed close to the

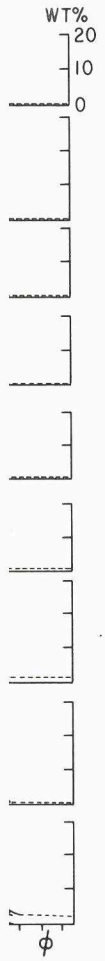


an diameter ($Md_\phi$), Inman sorting coeffi-
(unornamented) and lithics (*solid*) for nine
dale, 1971)

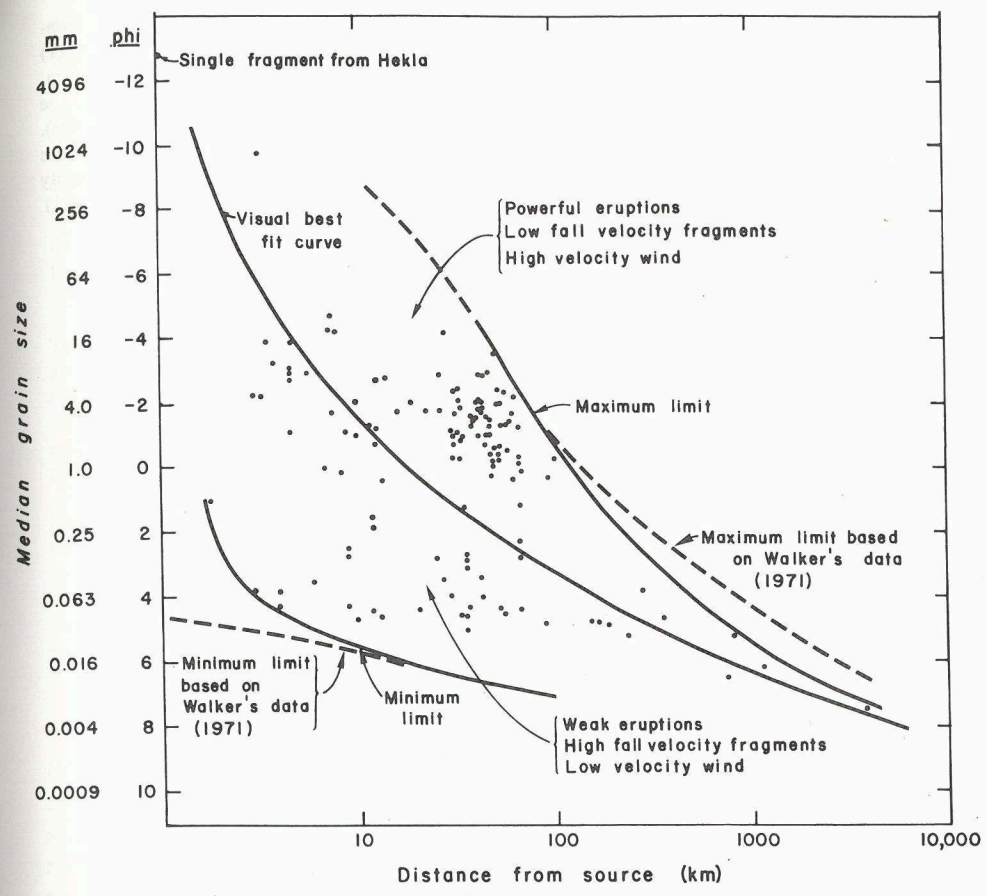


**Fig. 6-36.** Median diameter ($Md_\phi$) plotted against distance from source for various tephra sheets. (After Fisher, 1964b; Walker, 1971)

'alker (1971), it appears that most
:en 1 and 2, with most around 1.4.
; distance from the vent (Fisher,
:xample, small-particle agglutina-
ıentation of fine-grained material
ın, 1982). And, at small distances
size), sorting values may increase
roasdale, 1971; Suzuki et al., 1973;
ew kilometers from the vent is due
nice, crystals, and rock fragments.
:er and Croasdale, 1971) the grain
and positively skewed close to the

source, but becomes bimodal (mode between $0.0_\phi$ and $1.0_\phi$) at about 16.5 km from the source. The modes closer to the source are dominated by pumice, while those at large distances are dominated by sanidine crystals (Fig. 6-37).

Another factor influencing sorting is the relative increase in density of pumice with decreasing grain size, owing to the decrease of the ratio of vesicle volume to the volume of actual glass. Thus, at very small grain sizes (depending on vesicle size and degree of vesiculation), densities of glass, lithic and felsic crystals become similar.

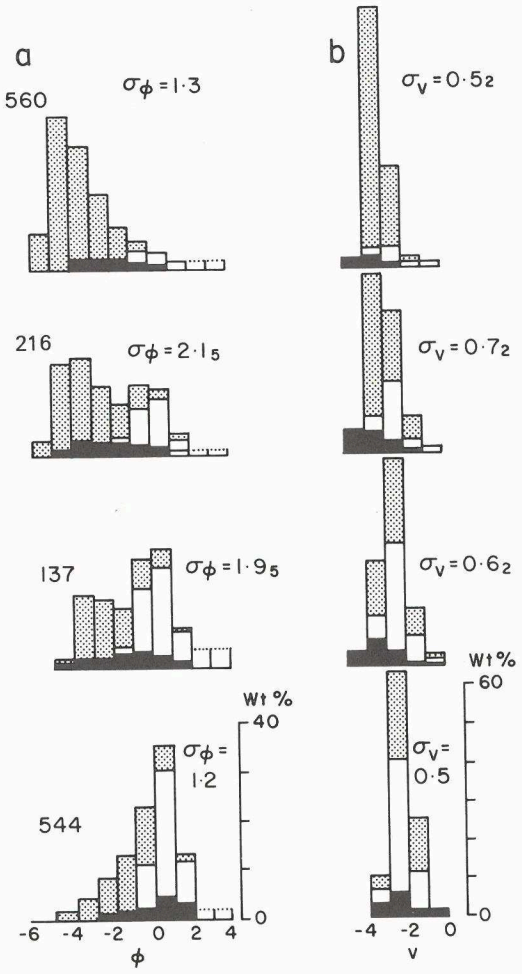


**Fig. 6-37 a, b.** Variation in pumice (*stippled*), crystals (*blank*) and lithics (*block*) for four samples from Fogo A tephra, Azores. Sample 560 is from nearest the vent (5.0 km) and 544 farthest (16.5 km). In histograms *b*, weight percentages are plotted against a function of fall velocity instead of grain size. (After Walker, 1971)

## Eolian Fractionation

Long ago, Murray and Renard (1884, p. 478) (also see Judd, 1888, p. 40) pointed out that the andesitic tephra nearest to the 1883 Krakatau eruption was more mafic than farther away. They suggested that differences in settling velocity between crystals and glass shards were the main cause – the denser crystals settling first, and the more silicic, less dense glass shards and pumice being carried farther away, possibly because they went higher and therefore were carried farther downwind. This same explanation is given for downwind changes in composition of the fallout ash from May 18, 1980 Mount St. Helens ash (Sarna-Wojcicki and Meyer et al., 1981), which shows downwind increases in $SiO_2$, $K_2O$ and decreases in $Al_2O_3$, CaO, and $TiO_2$ from bulk samples.

Larsson (1937), who compared the bulk chemical composition of ash from three widely spaced samples from the 1932 eruption of Quizapu Volcano, Chile,

**Fig. 6-37 a, b.** Variation in pumice (*stippled*), crystals (*blank*) and lithics (*block*) for four samples from Fogo A tephra, Azores. Sample 560 is from nearest the vent (5.0 km) and 544 farthest (16.5 km). In histograms *b*, weight percentages are plotted against a function of fall velocity instead of grain size. (After Walker, 1971)

with lapilli deposited near the source, noted that near-source lapilli were andesitic to dacitic (about 64% $SiO_2$), whereas ash became more silicic with increasing distance from the source (Table 6-4), the most "differentiated" sample having about 70% $SiO_2$. He attributed the increase in $SiO_2$ content to a progressive loss of crystals (plagioclase, hornblende, pyroxene, apatite, magnetite) which contain less silicon than the glass. Larsson called this process of chemical change with distance in volcanic ash *eolian differentiation*. We prefer the term *eolian fractionation* of Lirer et al. (1973) to emphasize that different types of components in a particulate system can be fractionated relative to each other.

**Table 6-4.** $SiO_2$ Content, distance from source and original composition (lapilli), Quizapu ash (Larsson, 1937)

| Analyzed material | Distance (km) | $SiO_2$ (wt. %) |
|---|---|---|
| Lapilli | 85 | 63.8 |
| Lapilli | 85 | 64.6 |
| Ash | 230 | 67.5 |
| Ash | 1,120 | 69.8 |
| Ash | 780 | 70.2 |

An assessment of eolian fractionation must distinguish three sets of variables: (a) magma chamber variables; (b) eruption column variables; and (c) transfer system variables. Most large silicic-alkalic magma chambers, for example, are compositionally zoned both chemically and mineralogically (composition and types, ratios and volumes of mineral phases). Moreover, the products are commonly erupted in order of their position in the magma column, proceeding from silicic to more mafic in both Plinian fallout and pyroclastic flow eruptions, as is shown in the deposits. In some cases the more mafic parts of such a zoned eruptive phase are distributed farther (Lirer et al., 1973), whereas in others they are confined near the volcanic source (Bogaard, 1983). Thus, studies of eolian fractionation must assess progressive lateral as well as temporal vertical changes, keeping in mind the possibility of compositionally heterogeneous magma chambers.

Although dynamic processes within eruption columns are poorly known, several workers have noted that crystals are commonly enriched in pyroclastic flow deposits because the vitric lighter components are winnowed out, that is, fractionated during upward rise, collapse, and dispersal of the eruption column, and also during transport (Hay, 1959a; Lipman, 1967; Walker, 1972a; Sparks and Walker, 1977). Thus, the bulk composition of fallout tephra associated with pyroclastic flows at any single locality (co-ignimbrite airfall tephra) does not truly represent the composition of the original magma.

Fractionation within a traveling ash cloud results from settling velocity differences of crystals, small pumice particles, glass shards and rock fragments. Their modal size distribution in the deposits is also determined by the initial size distribution in the magma chamber or eruption column. In any case, bulk chemical analyses of samples from fallout layers is not very useful for studies of original magma

**Table 6-5.** Fragment percentages, calculated ratios and size parameters with respect to distance for 1919 Kelut ash samples (Java). Percentages of fragmental components are determined for total of sample fractions in the following grade sizes: 2–1 mm, 1.0–0.5 mm, 0.5–0.2 mm, 0.2–0.1 mm, and 0.1–0.05 mm (Atterberg scale) (Baak, 1949, Table 9). $Md_\phi$ and $\sigma_\phi$ were determined from curves drawn from Baak's (1949) data on his Table 8 for total samples

| Sample No. | Distance (km) | Relative percentage of fragments | | | | | Ratios | | Size parameters (whole samples) | |
|---|---|---|---|---|---|---|---|---|---|---|
| | | Op.[b] | Fm.[c] | Plag. | Lithic | Shards | Op./Op.+Fsp. | Lithic/glass | $Md_\phi$ | $\sigma_\phi$[d] |
| [a] | 36 | 6 | 13 | 51 | 13 | 18 | 0.11 | 0.72 | 3.29 | 1.80 |
| 7038 | 43 | 5 | 7 | 45 | 10 | 33 | 0.10 | 0.30 | 3.90 | 1.38 |
| 8561 | 56 | 2 | 8 | 48 | 8 | 34 | 0.04 | 0.24 | 4.40 | 1.60 |
| 7050 | 66 | 8 | 9 | 56 | 12 | 18 | 0.13 | 0.66 | 4.30 | 1.61 |
| 8272 | 154 | 4 | 8 | 43 | 9 | 36 | 0.09 | 0.25 | 4.65 | 1.30 |
| 7039 | 166 | 15 | 5 | 39 | 7 | 34 | 0.28 | 0.21 | 4.68 | 1.28 |
| 7042 | 4 | 6 | 9 | 38 | 13 | 34 | 0.14 | 0.38 | 4.25 | 2.10 |
| 7046 | 9 | 6 | 13 | 54 | 15 | 12 | 0.10 | 1.25 | 2.70 | 1.82 |
| 7043 | 36 | 3 | 11 | 27 | 12 | 43 | 0.10 | 0.28 | NA[e] | NA |
| 8501 | 92 | 3 | 7 | 27 | 9 | 54 | 0.10 | 0.17 | 4.70 | 1.30 |
| 8271 | 360 | 19 | 6 | 44 | 4 | 27 | 0.30 | 0.15 | 4.55 | 0.53 |

[a] Average of four samples: Nos. 7049, 8503, 8506, 8505
[b] Op. = opaque oxides, Fsp. = Feldspar
[c] Fm. = Ferromagnesian minerals (augite, hypersthene, green and brown hornblende)
[d] Phi ($\phi$) = $-\log_{2\phi}$ in mm; $\sigma_\phi = 84_\phi - 16_\phi/2$ (Inman, 1952). NA = not determined
[e] NA = not analyzed

compositions; it is necessary to know the size and distribution of different components, prior to detailed chemical analyses by microprobe and other methods. The composition of glass within ash, however, represents the composition of the liquid fraction at the time of eruption.

Minerals are generally most abundant between about 2 mm ($-1_\phi$), and 1/16 mm ($4_\phi$) and are practically absent below about 10 μm, whereas glass shards can be much smaller. An ash-fall deposit from a homogeneous magma batch should therefore become increasingly silicic with distance because the interstitial liquid of a magma is generally more silicic than the crystals, except, of course, for quartz.

Minerals and glass shards in ash samples from the 1919 eruption of Kelut volcano (Java) showed the following trends (Table 6-5): lithic fragments, amphibole, pyroxene, and feldspar crystals decrease in size and amount away from the source relative to glass shards and opaque minerals (dominantly magnetite). The relative increase in glass shards is apparently the reason for an increase in silica content of the bulk ash, despite a relative increase in opaque oxide minerals. Although feldspar tends to decrease in absolute amount with distance from Kelut, the grade size between 0.1 mm and 0.02 mm usually contains the largest volume of feldspar in any given sample (Table 6-6) reflecting primary size fractionation during dispersal. At the same time, the size of feldspar in any given sample (Table 6-6) reflects only the primary size of phenocrysts in the magma prior to eruption. The total volume of feldspar crystals decreases with distance in the coarser fractions, but remains about the same in the finer fractions.

Although the settling velocities of heavy and light minerals differ significantly, Kittleman (1973) shows that their relative proportions in Mazama ash does not change significantly with distance up to 400 km from the source, even though grain size of the samples decreases from a median diameter of $-4_\phi$ to $-5_\phi$ near the source to about $2_\phi$ at about 200 km (Fig. 6-38). This rather puzzling feature has not been ex-

**Table 6-6.** Volume percent feldspar crystals, 1919 Kelut ash. Figures in italics are maxima. (Data from Baak, 1949, Table 11)

| | Distance (km) | Grade size (mm) | | | |
|---|---|---|---|---|---|
| | | 0.5–0.2 | 0.2–0.1 | 0.1–0.02 | 0.02–0.05 |
| East of Kelut | 36 | *12.0* | 11.0 | 10.0 | 3.5 |
| | 36 | *13.0* | 10.0 | *14.0* | 4.3 |
| | 36 | 7.5 | 12.2 | *14.0* | 2.2 |
| | 36 | –0– | 8.3 | *16.0* | 1.7 |
| | 43 | 3.5 | 6.0 | *13.0* | 3.3 |
| | 56 | 7.8 | 7.5 | *12.0* | 3.5 |
| | 66 | 8.8 | *10.0* | 9.3 | 3.8 |
| | 154 | –0– | 5.7 | *16.3* | 2.0 |
| | 166 | –0– | 2.3 | *15.0* | 4.3 |
| West of Kelut | 4 | *10.0* | 8.5 | 9.0 | 3.3 |
| | 9 | 11.5 | 11.5 | *12.2* | 2.5 |
| | 36 | 4.0 | 9.0 | *12.0* | 3.0 |
| | 92 | –0– | 3.7 | *11.7* | 4.0 |
| | 360 | –0– | –0– | *19.0* | 4.5 |

[a] Up. = opaque oxides, Fsp. = Feldspar
[c] Fm. = Ferromagnesian minerals (augite, hypersthene, green and brown hornblende)
[d] Phi ($\phi$) $= -\log_{2\phi}$ in mm; $\sigma_\phi = 84_\phi - 16_\phi/2$ (Inman, 1952). NA = not determined
[e] NA = not analyzed

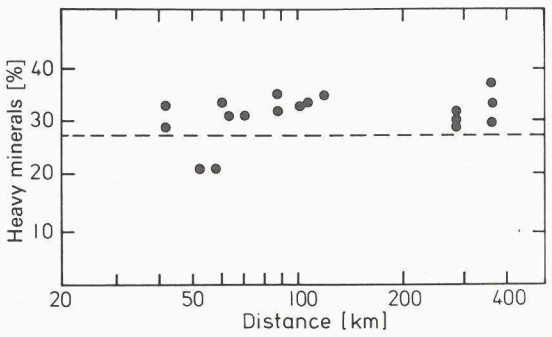


**Fig. 6-38.** Percent heavy minerals among free crystals in Mazama fallout tephra plotted against distance from source. *Dashed line* is percentage of heavy minerals among crystals enclosed in pumice. (After Kittleman, 1973)

plained and requires further study. Other data indicating that eolian fractionation is not a simple issue come from the 1947 eruption of Hekla, where silica percentage of glass shards did not vary significantly with distance despite a difference in $SiO_2$ content between the earliest erupted, brownish-gray tephra and the closely following and more mafic, brownish-black tephra during the continuous eruption (Table 6-7).

One of the most complete studies of eolian fractionation is on the Recent White River ash in Alaska and Canada (see Fig. 6-11) (Lerbekmo and Campbell, 1969; Lerbekmo et al., 1975) that originally extended over an estimated area of > 300,000 $km^2$ and had a minimum volume of about 25 $km^3$ (Fig. 6-39). The chemical com-

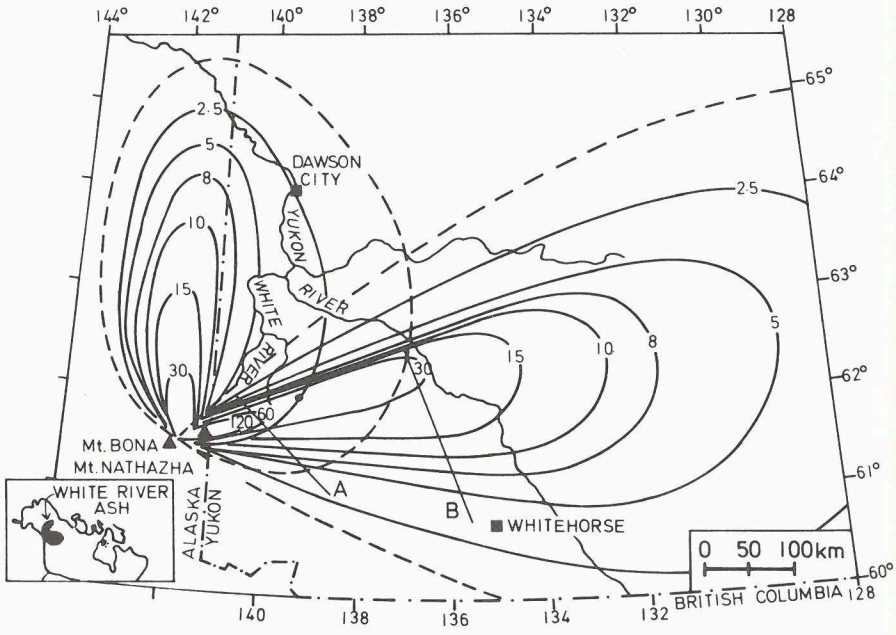


**Fig. 6-39.** Isopach map of the two lobes of White River ash. Lines A (west) and B (east) are approximate locations of traverses for data in Fig. 6-40 and Table 6-8. (After Lerbekmo and Campbell, 1969; Lerbekmo et al., 1975)

**. 6-38.** Percent heavy minerals ong free crystals in Mazama fallout hra plotted against distance from rce. *Dashed line* is percentage of avy minerals among crystals enclosed pumice. (After Kittleman, 1973)

ating that eolian fractionation Hekla, where silica percentage ce despite a difference in $SiO_2$ tephra and the closely follow- ne continuous eruption (Table

onation is on the Recent White erbekmo and Campbell, 1969; an estimated area of >300,000 (Fig. 6-39). The chemical com-

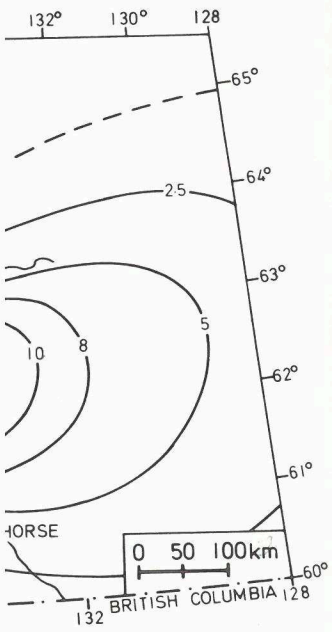


es A (west) and B (east) are approximate Lerbekmo and Campbell, 1969; Lerbek-

**Table 6-7.** $SiO_2$-variation with distance, 1947 Hekla (Iceland) brown-grey and brown-black tephra compared with original composition (bomb). (Data from Thorarinsson, 1954, Plate 2, Table 8)

| Analyzed material | Distance (km) | $SiO_2$ |
|---|---|---|
| Brown-gray bomb | – | 60.9 |
| Brown-gray tephra | 32 | 61.9 |
| Brown-gray tephra | 50 | 61.7 |
| Brown-gray tephra | 70 | 61.5 |
| Brown-black tephra | 4 | 56.3 |
| Brown-black tephra | 6 | 57.5 |
| Brown-black tephra | 32 | 57.7 |
| Brown-black tephra | 283 | 57.1 |
| Red-brown dust | 3,800 | 56.4 |

**Table 6-8.** Averages of chemical analyses of ash samples collected from two traverses 190 km apart across east lobe of White River ash, Yukon Territory, Canada (Lerbekmo and Campbell, 1969)

| Traverse A | | Traverse B | |
|---|---|---|---|
| Western (proximal) traverse (mean of samples 30–46, 66) | | Eastern (distal) traverse (mean of samples 1–27) | |
| | wt. % | | wt. % |
| $SiO_2$ | 62.2 | $SiO_2$ | 70.2 |
| $Al_2O_3$ | 17.8 | $Al_2O_3$ | 13.9 |
| MgO | 2.5 | MgO | 1.6 |
| $Na_2O$ | 5.2 | $Na_2O$ | 3.9 |
| $K_2O$ | 1.9 | $K_2O$ | 2.8 |
| CaO | 6.3 | CaO | 3.3 |
| FeO | 2.1 | FeO | 2.2 |
| $Fe_2O_3$ | 1.5 | $Fe_2O_3$ | 1.5 |
| $TiO_2$ | 0.5 | $TiO_2$ | 0.5 |
| (Rb | 21 ppm) | (Rb | 39 ppm) |
| (Sr | 1,269 ppm) | (Sr | 624 ppm) |
| K/Rb | 762 | K/Rb | 589 |
| Ca/Sr | 35 | Ca/Sr | 38 |

position of samples from two traverses 190 km apart across the east lobe shows large differences in the first six oxides and in Rb and Sr (Fig. 6-40, Table 6-8). The differences are interpreted as caused by an increase in glass relative to the crystal components as a function of size and distance from the source. The spread of values around the best-fit curves at equal distances (Fig. 6-40) is probably because many samples were collected off the main dispersal axis.

In a later, more detailed mineralogical study, Lerbekmo et al. (1975) noted that the age of the northern lobe is about 1887 years B.P. while that of the eastern lobe is 1250 years B.P. Although the chemical composition of glass and most pheno-

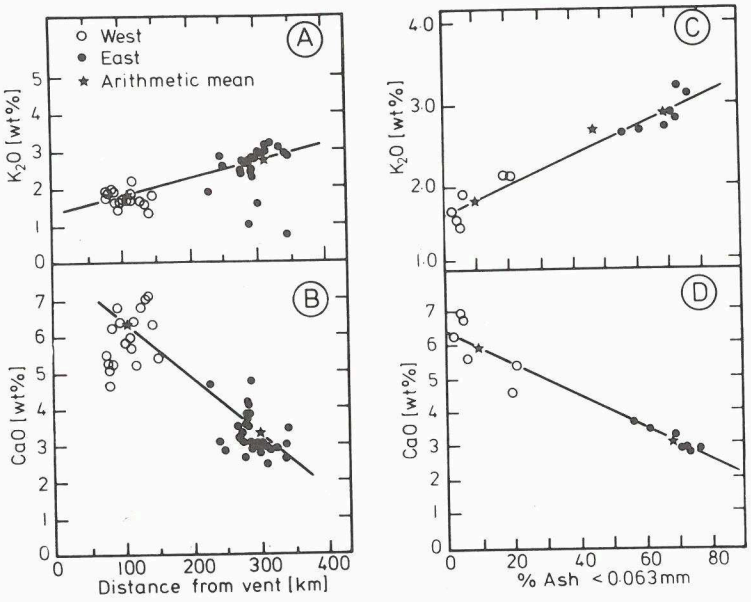


**Fig. 6-40 A–D.** $K_2O$ and CaO contents versus distance from vent for traverses **A** and **B** (in Fig. 6-39) across east-trending lobe of White River ash. **C** $K_2O$ versus grain size for east and west traverses across east-trending lobe. **D** CaO content for same samples as in **C**. (After Lerbekmo and Campbell 1969)

crysts is identical in the two lobes, there are significant differences in ilmenite composition (particularly Fe, Ti, and Mg). Calculated temperatures of crystallization and oxygen fugacities from the composition of co-existing magnetites and ilmenites suggest that magmas supplying ash for the northern, older lobe crystallized at about 830° to 1005 °C while those from the younger eastern lobe had higher temperatures (about 1035° to 1125 °C). Curiously, temperatures calculated from mineral composition in vertical sections of the northern lobe ash show a decrease with time and distance indicating that higher temperature magmas (from a zoned magma chamber?) were erupted first, whereas lower temperature magmas were erupted last and the products transported farther from the source.